



**HAL**  
open science

## Pluriannual beach-dune evolutions at regional scale: Erosion and recovery sequences analysis along the aquitaine coast based on airborne LiDAR data

Alexandre Nicolae Lerma, Bruce Ayache, Beatrice Ulvoas, François Paris,  
Nicolas Bernon, Thomas Bulteau, Cyril Mallet

### ► To cite this version:

Alexandre Nicolae Lerma, Bruce Ayache, Beatrice Ulvoas, François Paris, Nicolas Bernon, et al..  
Pluriannual beach-dune evolutions at regional scale: Erosion and recovery sequences analysis along  
the aquitaine coast based on airborne LiDAR data. Continental Shelf Research, 2019, 189, pp.103974.  
10.1016/j.csr.2019.103974 . hal-02413837

**HAL Id: hal-02413837**

**<https://brgm.hal.science/hal-02413837>**

Submitted on 20 Jul 2022

**HAL** is a multi-disciplinary open access archive for the deposit and dissemination of scientific research documents, whether they are published or not. The documents may come from teaching and research institutions in France or abroad, or from public or private research centers.

L'archive ouverte pluridisciplinaire **HAL**, est destinée au dépôt et à la diffusion de documents scientifiques de niveau recherche, publiés ou non, émanant des établissements d'enseignement et de recherche français ou étrangers, des laboratoires publics ou privés.



Distributed under a Creative Commons Attribution - NonCommercial 4.0 International License

1 **Pluriannual beach-dune evolutions at regional scale: Erosion and recovery**  
2 **sequences analysis along the Aquitaine coast based on airborne LiDAR data**

3 Authors: Alexandre Nicolae Lerma, Bruce Ayache, Beatrice Ulvoas, François Paris, Nicolas Bernon,  
4 Thomas Bulteau, Cyril Mallet

5 Corresponding author: a.nicolaelerma@brgm.fr

6 Affiliation: BRGM (French Geological Survey), Direction Régionale Nouvelle-Aquitaine, Parc  
7 Technologique Europarc, 24 avenue Léonard de Vinci, 33600 Pessac, France,

8

9 **Abstract:**

10 With apparent uniformity, the 230 kilometers of the Aquitanian sandy coast presents many differences  
11 in geomorphological characteristics and evolutions at the event, seasonal, annual and pluriannual time  
12 scales. This contribution highlights work based on extensive airborne LiDAR coverage campaigns  
13 realized in 2011, 2014, 2016 and 2017. Geomorphological evolutions are studied at the scale of the  
14 sedimentary cell and subcells of the Aquitanian sandy coast, specifically through the automatic detection  
15 of dune erosion scarps and incipient foredunes, the planimetric indicators of foredunes, dune feet and  
16 dune front evolutions along the coast, and the sediment budget of the beach-dune interface. Analyses  
17 were performed for two periods: 2011-2014 (including the erosional impact of the 2013-2014 winter)  
18 and 2014-2017, presenting continuous and extensive beach recovery at the beach-dune interface. Dune  
19 erosion scarps and incipient foredune characteristics are analyzed in term of alongshore length, width,  
20 surface and shape. A classification based on the alongshore length of the erosion scarp shows great  
21 diversity of erosional dynamics, which are directly linked to the geomorphologic characteristics of the  
22 beach sediment availability and the nearshore bar system. This diversity includes homogeneously large  
23 erosional bands above a 1 km alongshore length, periodic Mega cusp embayments from 200 to 800 m,  
24 and a local erosion mark less than 200 m long. Analysis for the following period shows a prompt and  
25 massive recovery at the upper beach and dune foot proxies on the majority of the coast. However, the  
26 recovery process as well as erosion is strongly marked by a North–South gradient. The dune front was  
27 massively impacted in Gironde, with a retreat exceeding 25 m that was poorly prograded since 2014,  
28 whereas in Landes a progradation of the front dune is observed compared to 2011. During the first period  
29 (including the 2013-2014 winter), more than  $15\,500 \times 10^3 \text{ m}^3$  of sediment was eroded from the beach-  
30 dune interface, which represents on average a loss of  $66 \text{ m}^3$  per linear meter. The gains during the  
31 following period (2014-2017) are also massive, above  $13\,500 \times 10^3 \text{ m}^3$ , with an average gain of  $57 \text{ m}^3$   
32 per linear meter. Given the budget between the two periods, 86.5 % of the sand eroded in 2014 had  
33 moved back in 2017 at the beach-dune interface but was generally further south following the dominant  
34 north-south alongshore drift. At the pluriannual, decadal and pluridecadal scales, the different sections  
35 of the coast follow various trends concerning erosion as well as recovery processes.

36 **Key words:** Airborne LiDAR, beach-dune interface, massive erosion, erosion scarp, pluriannual  
37 recovery, incipient foredune, sediment budget

38

39

40

## 41 Introduction

42 Beach-dune systems as an interface between the marine and terrestrial environments constitute a buffer  
43 zone against marine hazards. Dune retreat is generally the consequence of major storm events and  
44 characterizes the erosion hazard. Dunes are also considered as the first line of defense against flooding.  
45 Over many years, evolutions of the dune front during storm conditions were observed and analyzed in  
46 many places around the world (e.g., [Vellinga, 1982](#), [Pye and Neal, 1994](#); [Sallenger, 2000](#); [Esteves et al.,](#)  
47 [2012](#); [Almeida et al., 2012](#); [Houser, 2013](#); [Splinter et al., 2014](#); [Palmsten et al., 2014](#); [Dissanayake et](#)  
48 [al., 2015](#); [Castelle et al., 2015](#)). More recently, observations and analyses of the factors of post storm  
49 dune recovery have been a subject of increasing attention ([Matias et al., 2004](#); [Houser and Hamilton](#)  
50 [2009](#); [Vousdoukas et al., 2012](#); [Scott et al., 2016](#); [Castelle et al., 2017](#)). Recovery processes have been  
51 analyzed at various time scales from days ([Wang et al., 2006](#); [Coco et al., 2014](#); [Aungnuureng et al.,](#)  
52 [2017](#); [Segura et al., 2018](#)) to months ([Senechal et al., 2015](#); [Phillips et al., 2017](#)), years ([Castelle et al.,](#)  
53 [2017](#), [Burvingt et al., 2017](#)), or decades ([Houser et al., 2015](#)).

54 Several techniques can be used to study beach-dune interfaces, but these techniques vary in terms of  
55 their applicability at different spatial and temporal scales. For example, d-GPS campaigns are still  
56 regularly used for event surveys (pre and post storm survey, [Biausque and Senechal 2018](#); [Castelle et](#)  
57 [al., 2017](#), [Brenner et al., 2018](#)) but are limited to small coastal sections (hundreds meters to few  
58 kilometers). UAV photogrammetric campaigns are increasingly used to survey dunes and beaches  
59 ([Gonçalves and Henriques, 2015](#); [Turner et al., 2016](#)). They provide useful information for studying  
60 seasonal evolutions and provide very high-resolution data, but they are nevertheless limited to a few  
61 kilometers in coverage; additionally, post-treatment processing is still complex, presenting variable  
62 vertical accuracy results.

63 In the past 20 years, LiDAR surveys have been routinely used to study coastal evolutions, quantitative  
64 beach morphology changes ([Sallenger et al., 2003](#)), dune morphodynamics and volumetric changes  
65 ([Andrews et al., 2002](#); [Woolard and Colby, 2002](#)) and even subtidal morphology with adapted sensors  
66 in clear coastal waters ([Irish and White, 1998](#); [Pastol, 2011](#); [Aleman et al., 2015](#)). Many studies have  
67 investigated coastal dunes using LiDAR. They focused on morphologic features or volumetric  
68 information over time (among many others, [Woolard and Colby, 2002](#); [Richter et al., 2013](#); [Keijsers et](#)  
69 [al., 2014, 2015](#)), storm morphological impacts ([Saye et al., 2005](#); [Houser et al., 2008, 2015](#), [Pye and](#)  
70 [Blott 2016](#), [Burvingt et al., 2017](#)) or foredune biogeomorphic interactions ([Keijsers et al., 2015](#); [Doyle](#)  
71 [and Woodroffe, 2018](#)).

72 Airborne LiDAR offers a useful solution for obtaining topographic information of coastal dunes and  
73 intertidal areas, providing post treatment, gridded 1–2 m spatial resolution DTMs, typically with a 15–  
74 20 cm vertical accuracy and potentially covering several hundred kilometers. They offer extensive data  
75 sets to analyze large-scale coastal evolutions ([Scott et al., 2016](#), [Burvingt et al., 2017](#)). Even if LiDAR  
76 campaigns are relatively expensive and are time consuming due to post treatments, annual repetition of  
77 this kind of survey at post winter or post summer periods provide very valuable data to study the spatial  
78 variability of storm impacts or recovery sequences along large continuous coastlines ([Houser et al.,](#)  
79 [2015](#)). LiDAR's large coverage area and relatively accurate 3D data also offer high potential for  
80 morphometric parameter definitions ([Woolard and Colby, 2002](#); [Saye et al., 2005](#); [Brock and Purkis](#)  
81 [2009](#); [Burvingt et al. 2018](#), [LeMauff et al., 2018](#)).

82 Poorly urbanized (less than 10 %) and presenting an almost continuous 230 km long open beach-dune  
83 system, the sandy Aquitaine Coast is globally affected by erosion. Since 1985, [Bernon et al., 2016](#) the  
84 coastline has retreated at 2.5 m/year on average in Gironde and at 1.7 m/year on average in Landes.  
85 However, along the Aquitaine coast, the erosion rate at the pluri-decadal scale ([Castelle et al., 2018](#)) and  
86 at the seasonal scale ([Bulteau et al., 2014](#)) can have high geographic variability.

87 The aim of this study is first to characterize the impact of the extremely active 2013-2014 winter at  
88 regional scale, as it represented the highest winter-mean wave energy level since at least 1948  
89 (Masselink et al., 2016). Second, the progressive recovery between 2014 and 2017 along the Aquitaine  
90 coast is analyzed. Erosion and recovery phases are characterized through automatic detection of the  
91 erosional dune scarp and incipient foredune. Beach-dune evolutions are also investigated through  
92 several cross-shore morphometric indicators and volumetric changes. Then, the 2011-2017 evolutions  
93 are analyzed for the coastline evolution and volumetric budget. The results are finally discussed, and a  
94 conceptual model of the recovery stages is proposed before drawing the conclusions.

## 95 2. Materials and Methods

### 96 2.1 Site

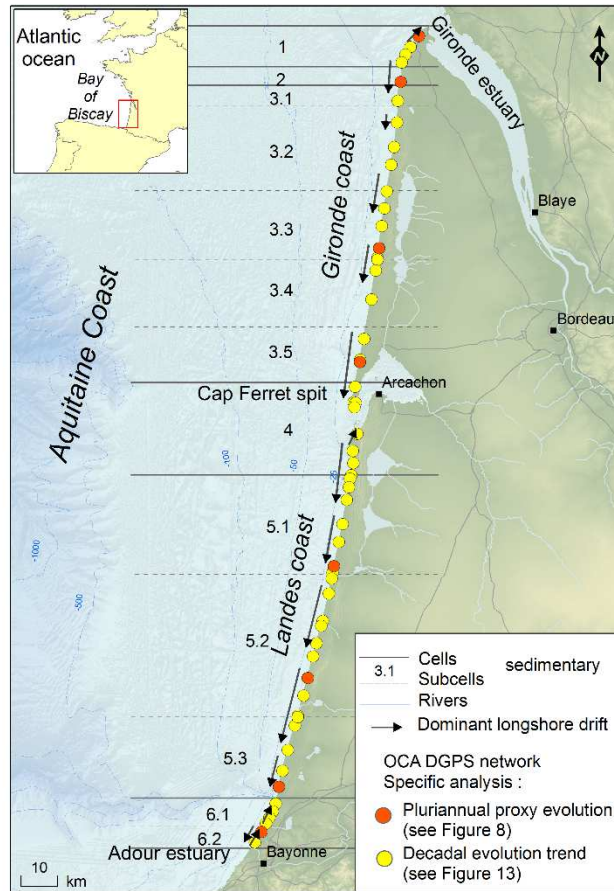
97 The sandy Aquitaine coast extends from the Gironde Estuary at the north to the Adour River at the south  
98 (Figure 1). It is an almost continuous 230 km long open beach-dune system (mainly interrupted by the  
99 inlet of the Arcachon lagoon). The continuous coastline of Gironde and Landes shows significantly  
100 different alongshore characteristics and was divided into relatively homogeneous sedimentary cells or  
101 subcells (Le Nindre et al., 2001; BRGM and ONF, 2017) based on several morphological and dynamic  
102 criteria; these criteria include the dominant longshore drift (Idier et al., 2013), nearshore sandbars  
103 configuration (Castelle et al., 2007), beach slope (Bulteau et al., 2016), sediment grain size (Pedreros,  
104 2000), seaward shelf width, beach width and the coastal dune system (BRGM and ONF, 2017) (Figure  
105 1). Table 1 synthetizes the main geomorphological characteristics of the nearshore and beach-dune  
106 interface along the coast, while a full description of the segmentation of the coast is detailed in BRGM  
107 and ONF (2017).

108 The coast is quite homogenously exposed to the Atlantic swell both annually (Castelle et al., 2017) and  
109 during extreme storm conditions (Nicolae Lerma et al., 2015). The annual offshore wave means are  
110 approximately 1.8 m and 11.5 s for significant wave height ( $H_s$ ) and peak period ( $T_p$ ), respectively.  
111 Extreme offshore  $H_s$  conditions defined here as 100-year return values are also quite similar, with a  
112 slight increase from north ( $H_s = 11$  m) to south ( $H_s = 11.6$  m) (Nicolae Lerma et al., 2015).

113 The mean wave directions are from the west in the northern part of the coast, whereas the directions are  
114 from the northwest in the south of the coast, explaining relatively to the orientation of the coast the  
115 general characteristics of the longshore drift (Idier et al., 2013) (Figures 1 and 2). Along the coast, the  
116 longshore drift is generally southward oriented except for Cell 1, and Cells 6.1 and 6.2 showed that the  
117 annual residual dominant direction is northward-oriented. Annual residual flux volumes estimated by  
118 Idier et al., 2013 are on average between 200 000 to 400 000 m<sup>3</sup>/y in Gironde, with a local substantial  
119 increase at the Cap Ferret spit with 657 000 m<sup>3</sup>/y. The residual flux in Landes decrease from Cell 4 to  
120 Cell 5.3 from 700 000 to 500 000 m<sup>3</sup>/y. At Cells 6.1 and 6.2, due to a change in the orientation of the  
121 coast and coarser sediment, the flux is reduced and the directions are more contrasted, as the residual  
122 flux is at 40 000 m<sup>3</sup>/y northward-oriented.

123 Wind orientation at the Aquitaine Coast is quite homogenous along the coast except at the extreme  
124 south, where offshore winds are overrepresented in comparison with the rest of the coast (Figure 2).  
125 Winter winds mainly come from the west whereas dominant spring and summer winds (from April to  
126 September) come from the northwest and north. Main constructive winds, which are prone to  
127 accumulating sand at the dune foot, mostly come from the north or south with velocity > 5 m/s  
128 respectively to the typical median grain size (0.03 mm). Relative to the main orientation of the coast,  
129 these directions allow longer fetches and thus a larger transport capacity. Westerly winds can also  
130 contribute to foredune growth, but only where the beach systems are the widest in the southern Gironde  
131 (Cells 3.5, 4) and Landes coasts (Cell 5.1 to 5.3). Previous studies have reported significant contribution  
132 of aeolian flux of sand to sediment mobility along the coast. In Gironde Froidefond and Prud'homme

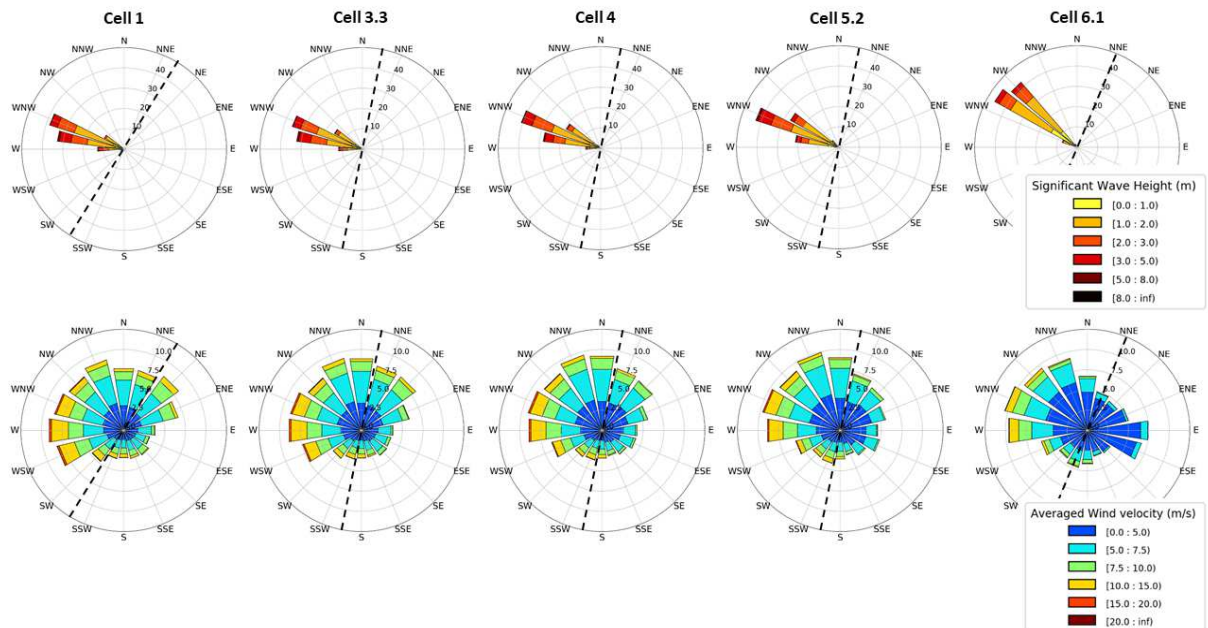
133 (1991) estimated the flux at 15 to 30 m<sup>3</sup>/m/yr before the fixation of the dune but Aubié and Tastet 2000  
 134 considered that aeolian sand loss moving landward is today almost negligible.



135

136

Figure 1: Location map



137

138 *Figure 2: General characteristics of significant wave height and means 10 m-wind conditions along*  
139 *the coast from 2008 – 2018 (hourly hindcast data, see section 2.3). Dashed black lines represent the*  
140 *coastline orientation at each sedimentary cell.*

141 *Table 1: Nearshore system and beach-dune main characteristics along the Aquitaine coast*

142 The first line dune along the Aquitaine coast is almost continuous and fixed. The human intervention on  
143 the dunes start at the half of the 19th century mainly through the plantation of ammophila arenaria used  
144 to stabilize the seafront dune system. Then, the dunes of the Aquitaine coast were progressively fixed,  
145 reprofiled and managed by the French National Forest Office ONF in the 1960s. Since then, no  
146 significant increase in the erosion rate was observed, which was attributed to the dune management  
147 performed by ONF (Castelle et al., 2018). However, the coastline evolution trends are geographically  
148 highly variable. Since 1985, coastline retreat rates are evaluated at 3.3 m/year in Nord Medoc (Cell 1)  
149 and 0.8 m/year in central Landes (sub-Cell 5.2 or 5.3) in Bernon et al. (2016). Strong variability was  
150 also observed at seasonal time scales, such as after the 2013-2014 winter, where field observations show  
151 in some areas a more than 25 m coastline retreat and in others no significant impact (Bulteau et al., 2014,  
152 Castelle et al., 2015).

153

## 154 2.2 Data

155 The main sources of data processed in this study are extensive coverage airborne LiDAR campaigns  
156 realized by the French National Geographic Institute (IGN) all along the Aquitaine coast. LiDAR  
157 campaigns were realized with synchronal orthophotography campaigns with a resolution of  
158 approximately 0.1 m. The control for data accuracy was realized in the raw data in which the density  
159 can vary between 2 and 8 points/m<sup>2</sup>. LiDAR data were controlled by comparing them with dedicated d-  
160 GPS data uniformly distributed along the coast (1550 points in unobstructed and flat surfaces on hard  
161 ground, such as parking, sports grounds, and roads). All campaign conformed to typical LiDAR  
162 accuracy ranges, with an absolute error of less than 20 cm (Table 2). The analysis presented in the study  
163 was realized on the 1 m horizontally gridded DTM in the French official altimetric reference called  
164 NGF/IGN69.

165 Apart from the 2011 campaign, which occurred just after the winter, all other campaigns occurred in the  
166 post-summer period and during approximately the same period before winter storm events (Table 2).  
167 Therefore, except for the 2011 campaign, beaches will show post-summer characteristics, thereby  
168 offering relevant information for interannual comparisons and avoiding seasonal bias.

169

170 *Table 2: LiDAR campaigns*

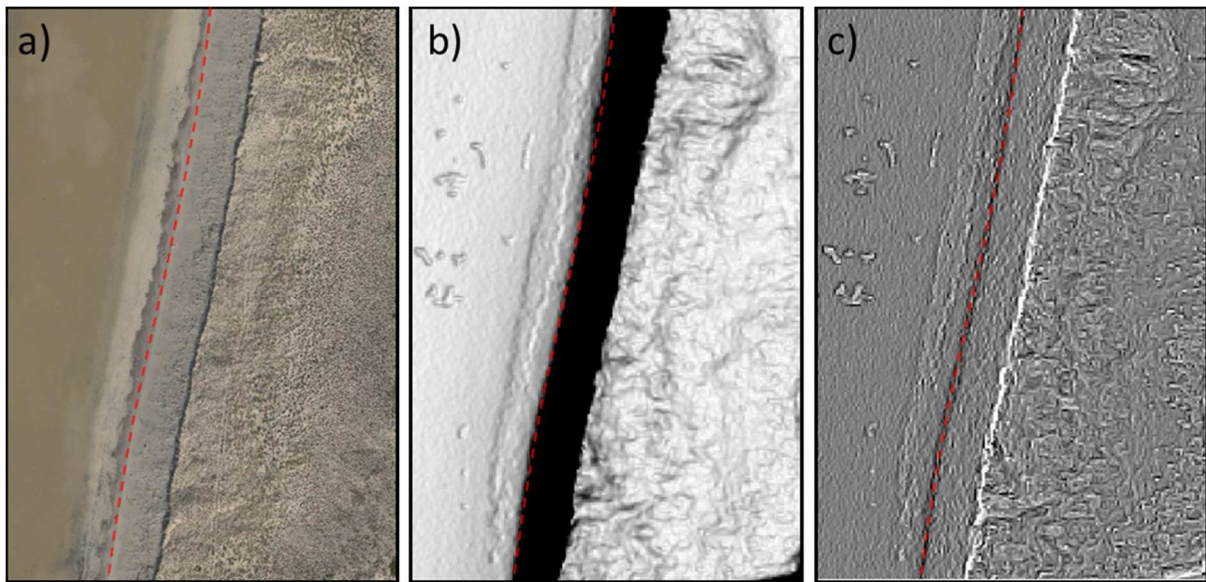
171

172 To complete an in-time LiDAR campaign analysis, data from annual post-winter d-GPS campaigns  
173 collected at 55 stations along the whole Aquitaine coast were exploited (Figure 1). Beginning in 2006,  
174 the Observatory of the Aquitane Coast (OCA) (see www.observatoire-cote-aquitaine.fr) has collected  
175 topographic transects annually based on a dedicated geodesic network implemented along the coast after  
176 the winter and the main storm erosive events. During these surveys, geomorphological descriptions of  
177 each profile were made to monitor the apparition or evolutions of incipient foredunes, beach scarps,  
178 pioneer vegetation, and evolutions of the frontier between the free dune (also called white dune), the  
179 grey dune and the forest.

180 The location and the spatio-temporal evolution of the coastline is also used to analyze LiDAR data.  
181 Many definitions of the coastline can be found in the literature (Boak and Turner 2005). The relevance

182 of one or another depends basically on their applications and the objective of each study. In our case, a  
183 practical definition based on geomorphologic criteria is used. The dune foot (Df) is defined as the slope  
184 break between the dune front and the upper beach or the foredune. The justifications to use this definition  
185 are multiple: (i) it allows an objective and common visual detection on the field, with orthophoto  
186 interpretation as automatic detection with GIS treatment (Figure 3), (ii) it enables detecting a limit whose  
187 evolution is in line with substantial erosion and recovery processes, (iii) it allows interpretations of  
188 seasonal and interannual evolutions.

189



190

191 *Figure 3: Tools for the dune foot location (dashed red line) as the coastline definition, a) Draped DTM;*  
192 *b) Slope map; c) Longitudinal curvature map.*

193

## 194 2.2 LiDAR treatment

### 195 2.2.1 Dune scarps, incipient foredune detection and beach-dune sand volume evolution

196 Part of the analyses are based on a GIS treatment dedicated on the one hand to detect automatically and  
197 delimitate massive beach scarps and associated eroded dune areas, and on the other hand, to detect  
198 established incipient foredunes directly in contact with the dune front (Figure 4).

199 Between two LiDAR campaigns, erosion scarps are defined as an altitude loss exceeding 3 m, directly  
200 in contact with the dune foot. These values were retained to exclusively consider massive erosion marks  
201 where the morphological impact was superior to the annual winter beach lowering (typically  
202 approximately 1.5 to 2 m). Several tests evaluated the applicability of lower values (2 m and 2.5 m).  
203 With a threshold smaller than 3 m, erosion pattern delimitations are noisier and are longshore-continuous  
204 in many parts of the coast, thereby not meeting a satisfactory analysis of erosion intensity. In contrast,  
205 incipient foredunes are altitude gains exceeding 1 m in direct contact with the dune foot. Incipient  
206 foredunes with inferior characteristics (several tens of centimeters) were not extracted mainly because  
207 with an accumulation under 1 m, foredune are hardly detectable on the field and were not considered as  
208 thoroughly established. For each kind of landform, a surface threshold of 500 m<sup>2</sup> is fixed to isolate only  
209 significant objects.

210 The altitude and thresholds used to define each kind of landform were compared and validated with  
211 observations taken during annual field campaigns along the coast and were based on synchronal photo  
212 interpretations made during the LiDAR campaigns.



213

214 *Figure 4: Photographs of the erosion dune scarp and foredune installation at the grand Crohot beach*  
215 *(Cell 3.4)*

216 To evaluate the main characteristics of erosion and recovery patterns along the coast, a classification of  
217 erosion and recovery is proposed based on their alongshore lengths as follows: Class 1 >800 m long;  
218 Class 2 from 400 to 800 m long; Class 3 from 200 to 400 m long; and Class 4 <200 m long.

219 Additionally, sediment budgets were calculated all along the coast using the dune foot of 2014 as the  
220 baseline. The budgets are calculated between 100 m seaward on the beach (near the Mean Sea Level)  
221 and 50 m landward on the dune starting from the dune foot (Figure 9). These limits were used to evaluate  
222 evolution at the beach-dune interface and limit the role of the intertidal zone variations, which can be  
223 substantial even at the tide cycle time scale. Complementary treatments consisting of isolated specific  
224 dune and upper beach erosion/accretion were made. On the basis of the differential volume of 2011-  
225 2014, the eroded volumes relative to the upper beach and to the dune were identified as being before  
226 and after the 2011 coastline, assuming that the coastline retreat observed in 2014 was mainly related to  
227 the 2013-2014 winter storm events. The same treatment occurred for the 2014-2017 period in  
228 considering the volumes before and after the 2014 coastline.

### 229 **2.2.2 Cross shore analysis of beach erosion and recovery**

230 On energetic open coasts, if small-scale morphology or sand levels can be highly variable at short time  
231 scales (day to weeks), the foredune and dune foot are considered as more established landforms (Hesp  
232 2002) that are affected only during main storm events.

233 Three altimetric proxies considered in reference to the French topographic datum (NGF-IGN69) are  
234 used to characterize the cross shore evolutions of the beach-dune interface, namely, the upper  
235 beach/foredune (4 m/NGF), the dune foot (6 m/NGF), and the dune front (10 m/NGF) (Figure 8). The  
236 temporal evolution of each proxy is analyzed along 1 km-spaced profiles perpendicular to the coast.  
237 This spatial resolution was considered as relevant for a regional scale analysis and is superior to potential  
238 periodic erosion marks observed along the coast, such as mega cusps.

239 The value of 4 m/NGF was retained because it corresponded in the major part of the studied profiles to  
240 the front of the incipient foredune, when this type of morphology is established and observable in the  
241 field (Figure 8). Due to the alongshore variability of beach slopes, sediment availability, and  
242 granulometry, these contour values can also be associated with the upper beach dynamic (erosion or  
243 accretion). However, taking into account that 4 m/NGF corresponds to 1 to 1.5 m above Highest

244 Astronomical Tide level, erosion at these contours should be related to highly energetic marine storm  
245 conditions and, conversely, accumulation morphologies are mainly related to wind driven dynamics.

246 For the dune foot, the value of 6 m/NGF corresponding to the alongshore and interannual average  
247 elevations (Nicolae et al., 2018) was used. As previously mentioned, the topography of the beach is  
248 variable from north to south, and the dune foot height varies between approximately 5 m at the north  
249 (Cell 1 and 2) to approximately 7 m at the south (Cell 6). Dune foot height at a certain location can also  
250 vary seasonally, being potentially exposed to winter storm erosion (lowering of the dune foot) and rapid  
251 sand accumulation related to favorable north-coming winds (rise of the dune foot). However, 6 m/NGF  
252 is meaningful and consistent for characterizing the evolutions of the beach-dune transition along the  
253 coast (Figure 8) at interannual and regional scales.

254 Finally, the dune front proxy located at 10 m/NGF directly characterizes the progradation or the retreat  
255 of the dune front all along the coast. Interpreting data just before a massive erosional event evolution of  
256 this proxy (typically progradation) can be related to the dune front sliding and slope regularization. This  
257 is not the case in our study, surveys having occurred after the summer season.

### 258 2.3 Hydrodynamical data

259 Hindcast hydrodynamic data are analyzed to characterize interannual and spatial variabilities at a  
260 seasonal time scale for water levels and wave energy along the coast. These data are currently used in  
261 the Aquitaine Early Warning System through synthetic indicators relating local storm surge conditions,  
262 wave conditions and geomorphological characteristics of the coast (Nicolae Lerma et al., 2018).

263 Tide and atmospheric surge data are collected from the MARC platform (Modelling and Analysis for  
264 Research in Coastal environment, [www.umr-lops.org/marc](http://www.umr-lops.org/marc)), and more precisely, from the structured  
265 domain covering the whole Aquitaine coast with a spatial resolution ( $\Delta d$ ) of 250 m. Data are extracted  
266 every 15 min for every 5 kilometers along the coast along the 10 m depth isobaths. The reference datum  
267 is the mean sea level (MSL), requiring a spatially variable vertical correction (RAM, 2016) to convert  
268 the results into the local topographic datum (IGN69).

269  
270 Wave data are also extracted from the MARC platform but from an unstructured domain with  $\Delta d$   
271 approximately 200 m at the coast. Data are extracted every 1 h along the 50 m depth isobath in front of  
272 the water level extraction point.

273  
274 Based on hourly data, two time series of daily maximum conditions at the center of the coast are  
275 presented in Figure 5. The time series are used here to characterize the relative intensity of the successive  
276 winters during the study period and linked the intensity to the erosion and recovery process.

277  
278 The wave energy flux per length unit of wave crest (noted  $P$ ) expressed in kW/m (Figure 5) was  
279 calculated in deep water according to the following equation (Tucker and Pitt 2001):

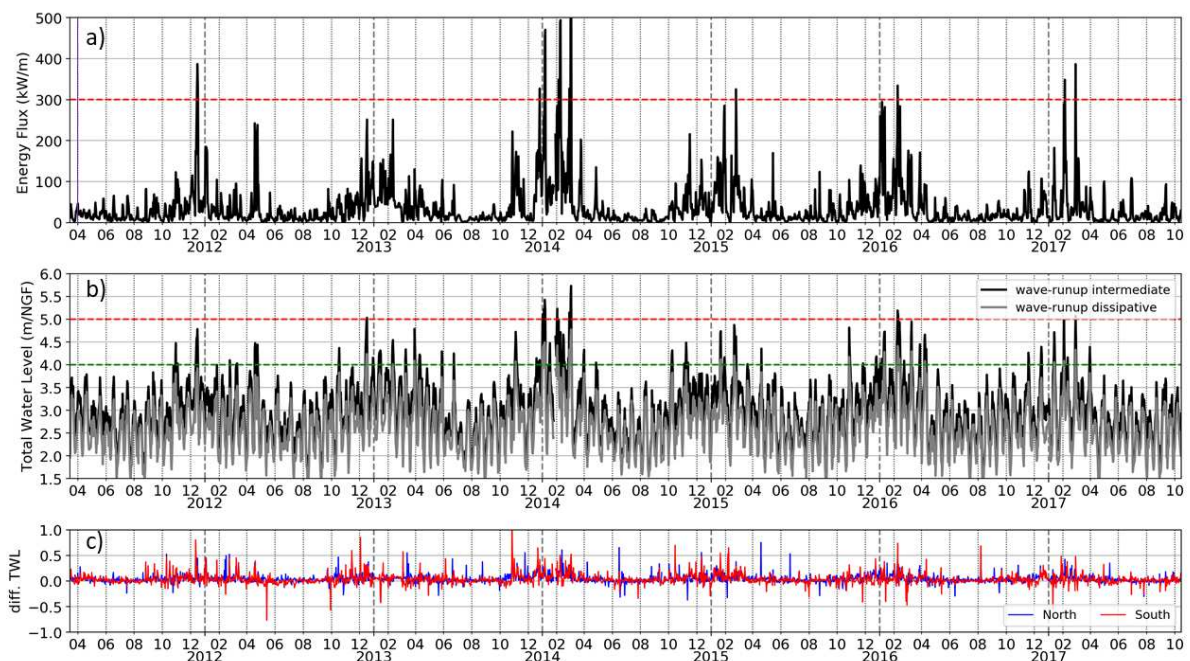
$$280 \quad P = \frac{\rho g^2}{64\pi} T_p H_s^2$$

281  
282 where  $\rho$  is the density of sea water, 1030 kg/m<sup>3</sup>;  $g$  is the gravitational acceleration, 9.81 m/s<sup>2</sup>;  
283  $H_s$  is the significant wave height; and  $T_p$  the peak period

284  
285 The Total Water Level (TWL) was calculated by summing the tide level, the atmospheric surge and the  
286 vertical runup (including wave setup and swash). The runup was estimated using  
287 two formulations developed by Stockdon et al. (2006) for intermediate and dissipative beaches. For the  
288 intermediate beaches, the slope parameter was set to 0.05 based on the typical mean upper beach  
289 profiles observed along the coast (Bulteau et al., 2016).

290

291 To illustrate the relative homogeneity of the forcing along the coast, the deviation of TWL for a point at  
 292 the north (Cell 3.2) and at the south (Cell 5.3) of the coast relatively to TWL at the center of the coast  
 293 (Cell 4) is illustrated (Figure 5). Differences in  $H_s$  for the same storm event are rarely above 1.5 m from  
 294 north to south (not shown). The tide level and atmospheric surge are also quite similar along the open  
 295 coast (excluding the Arcachon lagoon). Consequently, the variability at the scale of a storm event is  
 296 reduced by approximately 1 m maximum from north to south (Figure 5). The forcing is thus considered  
 297 as quite homogenous along the coast, and the alongshore variability of erosive impacts at the beach are  
 298 mostly related to sediment availability and associated morphological characteristics (nearshore bar  
 299 system, beach width, beach slope, and dune foot elevation, see Table 1)  
 300



301  
 302 *Figure 5: Daily maxima of forcing parameters along the coast between April 2011 and October 2017,*  
 303 *horizontal dashed lines represents thresholds in a) intense storm (wave criteria), Bulteau et al., 2019,*  
 304 *in b) green dashed line upper beach/foredune proxy, red dashed line lowest dune foot detected along*  
 305 *the coast.*

306

### 307 3. Results

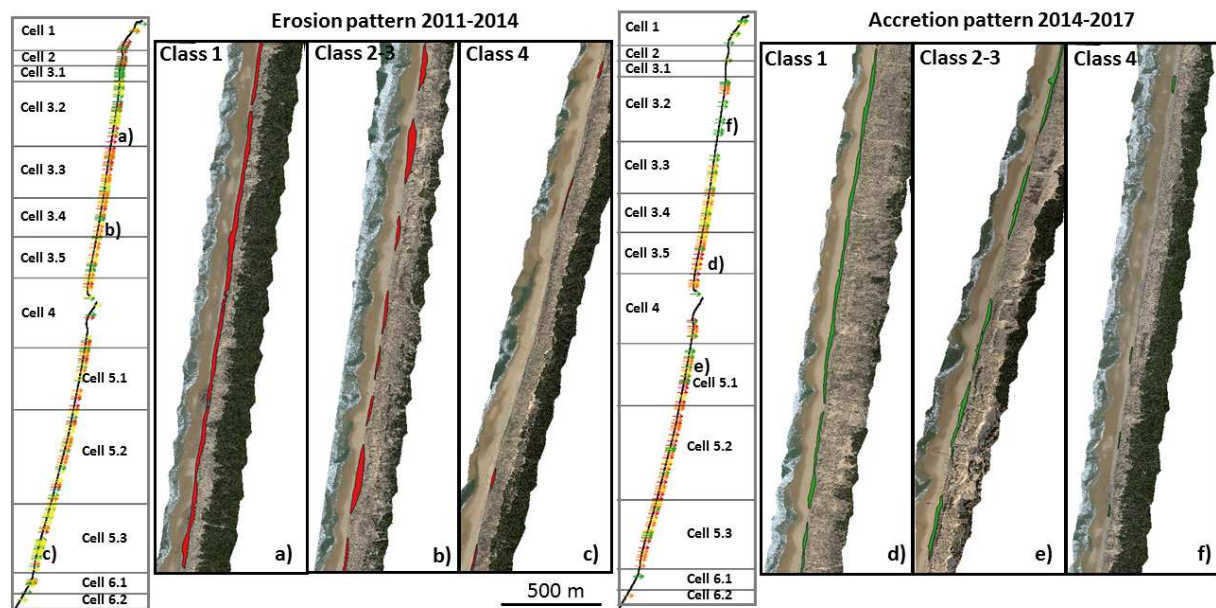
#### 308 3.1 Erosion characteristics after the 2013-2014 winter

##### 309 3.1.1 Dune scarp and beach erosion patterns

310 The automatic beach scarp detection indicates that almost all the coast was affected by substantial  
 311 erosion between 2011 and 2014. Along the coast, 255 erosion marks with a surface area above 500 m<sup>2</sup>  
 312 were detected along the coast. Erosion marks present variable characteristics between 16 to 3080 m long  
 313 and 4 to 44 m in width. The width of the erosion pattern was relatively homogenous along the coast  
 314 (between 11 and 24 m on average). Classification based on the alongshore length criteria was retained,  
 315 as it was more significant for analyzing the geographic repartition of each type of erosion pattern (Figure  
 316 6, Figure 7).

317 Erosion scarps detected in 2014 show great variability in shape along the coast. Due to a relatively  
 318 homogenous width, the main criteria used to classify the erosion marks is the alongshore dimension, but  
 319 erosion marks can also be analyzed in terms of shape (Figure 6). Class 1 characterizes continuous eroded  
 320 bands with quite homogenous cross-shore widths. This shape is expected to be observed on highly

321 exposed dissipative beaches with uniformly low-gradient intertidal beaches, unpronounced or longshore  
 322 uniform sand bars and low available sediment resources. The long-eroded bands are mainly observable  
 323 in North Gironde, where beaches show those characteristics.



324

325 *Figure 6:* Distribution of eroded dune scarps in 2014 (left panel) and foredunes in 2017 (right panel)  
 326 and an example of each class along the coast. In maps, crosses indicate erosion/accretion location, red  
 327 class 1, orange class 2, yellow class 3, green class 4. In orthophotos, red polygon delimits erosion  
 328 marks (left panel) and green incipient foredune (right panel).

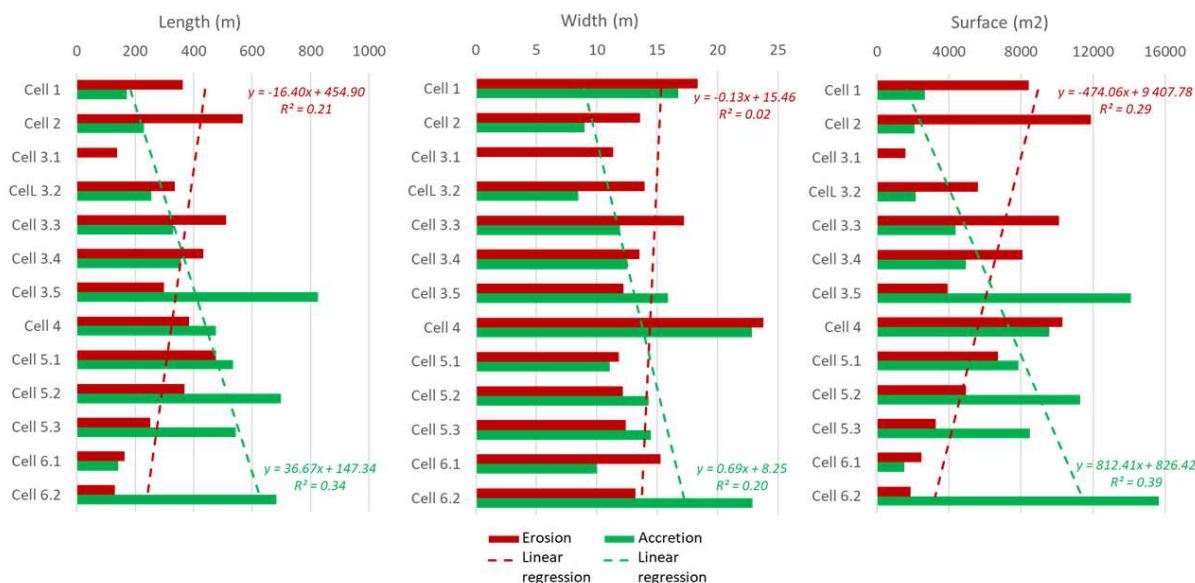
329 Classes 2 and 3 are cusp-shaped erosion scarps defined as a megacusps embayment (Thornton et al.,  
 330 2007; Castelle et al., 2015). The geometry of the megacusps are symmetric, with the center of the  
 331 embayment located roughly equidistant from its horns. The alongshore erosion differences during  
 332 storms such as mega cusps are related to nearshore bathymetry and particularly so with persistent rip  
 333 currents channels (Bender & Dean 2003; Schupp et al., 2006; Thornton et al., 2007; Houser et al., 2008,  
 334 Castelle et al., 2017). Rhythmic mega cusps are observable all along the coast but appear to have a  
 335 higher alongshore length in central and south Gironde compared to the Landes coast, where they are  
 336 more generally approximately 200 to 400 m in length (Class 3) (Figure 6). Finally, Class 4 corresponds  
 337 to local, generally also cusped, erosion marks or little scarps intercalated between the Class 1 shape.

338 Class 1 represents only 8.6 % of the number of erosional patterns detected but totals 55.6 % off of the  
 339 dune front eroded area. This pattern is representative of massive erosion, with a maximum of 44 m width  
 340 localized in Cell 4 at the south end of the Arcachon Lagoon pass. The maximum eroded surface reaches  
 341 676 555 m<sup>2</sup> localized in Cell 2.

342 In comparison, Classes 2, 3 and 4 respectively total 22.6 %, 16.4 % and 5.4 % of the eroded area.  
 343 Notably, for each class, the width of the erosion marks can vary from a few meters to more than 30 m.  
 344 Even if the erosion pattern of Class 4 is relatively small in the longshore direction, the width can be  
 345 substantial, with an average of 11.8 m and reaching more than 30 m in Cells 1 or 4, for example.

346 The spatial repartition of each class of erosion pattern is represented in Figure 6 and Figure 7. These  
 347 figures illustrate that erosional marks are observable all along the coast. We observe that the northern  
 348 coast's (from Cell 1 to 3.2) erosion marks are mostly characterized by Class 1 and Class 4 patterns.  
 349 Conversely, the central part of the coast, including the central and south part of the Gironde and Landes

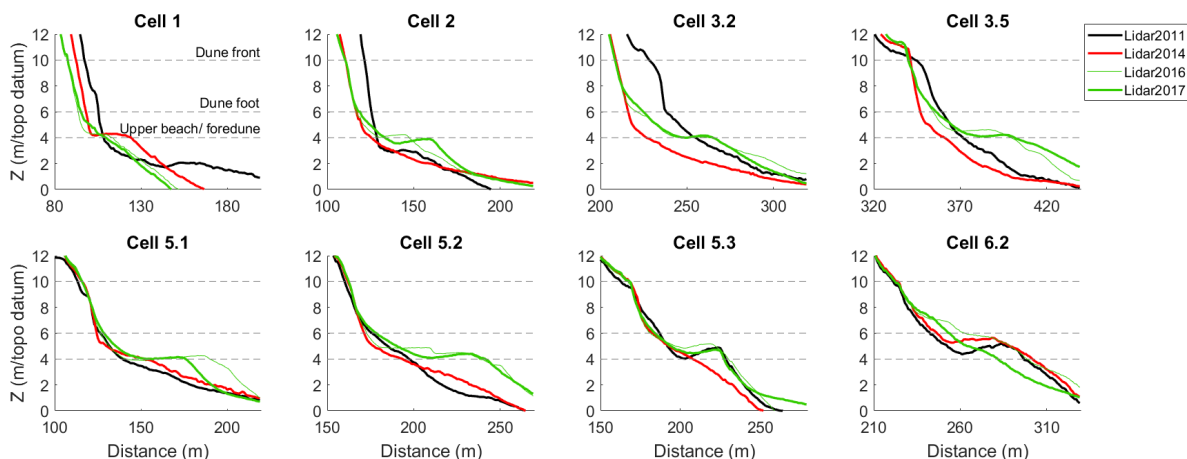
350 coasts (from Cell 3.3 to 5.3) are mostly characterized by Classes 2 and 3. Finally, the extreme south of  
 351 Landes (Cell 6 and 7) counts fewer erosion marks, and they are mostly from Class 4.



352  
 353 *Figure 7: Mean characteristics of dune scarps and accretion patterns along the coast, 2011-2014*  
 354 *period (red bar), 2014-2017 period (green bar).*

### 355 3.1.2 Cross shore beach-dune interface retreat

356 The retreat of the beach-dune system was very prominent almost all along the coast, except at the  
 357 extreme north end of Cell 1, at the direct proximity of the Arcachon inlet and at the extreme south of the  
 358 Landes (Cell 6.2), where progradation of the Df was observed. However, due to a local singularity due  
 359 to wave/tide interactions, hook ridge dynamics, or wave expositions, a planimetric retreat was  
 360 generalized between 5 and 20 m and beach lowering reached more than 2 m. The alongshore average  
 361 retreat is 6.5 m for the dune foot and 4 m for the dune front. Even if erosion is generalized, a north to  
 362 south gradient is observable, which is consistent with the previous classification of the erosion marks  
 363 (Figure 7). This dynamic is particularly observable considering the evolution of the dune front proxy.  
 364 The north (Cell 1) and the center of Gironde (Cell 3.2 and 3.3) were the most dramatically affected  
 365 areas, with massive retreats greater than 20 m (Figure 8 and 11). The south end of the Arcachon inlet  
 366 also observed brutal retreat, but it was much more local. Interestingly, the dune front was relatively  
 367 preserved in Landes (mostly Cells 5.1 and 5.2). Dune retreat was observed locally at the same order of  
 368 magnitude as in Gironde, but more generally, the dune front appears stable and some slight progradation  
 369 is even observable (Figure 8 and 11).



371 *Figure 8: Example of erosion and accretion at the altimetric proxies used in cross shore analysis along*  
372 *the coast*

373 In Landes, the situation is much more contrasted, with many locations presenting at least progradation  
374 at the Upper beach/Fordune proxy. This is related to rapid recovery at the upper beach during the month  
375 directly after the 2013-2014 winter.

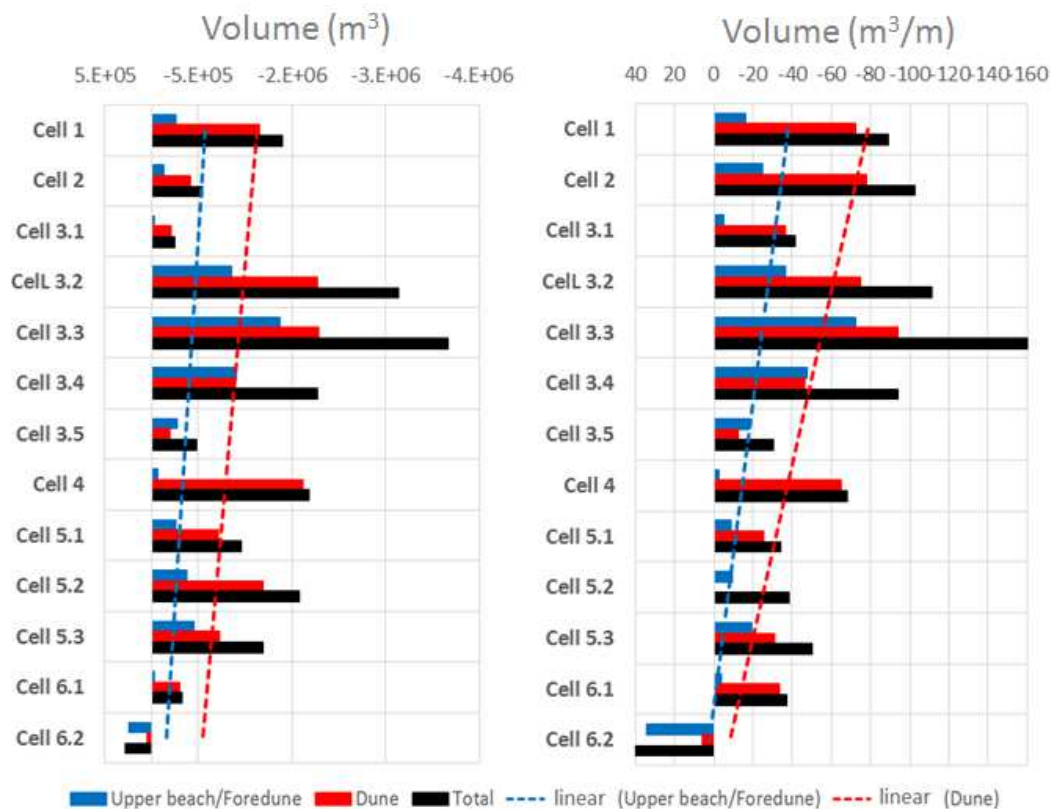
376 In Cell 6, we observe consolidations of the foredune that have not been significantly affected thanks to  
377 the specificities of beach-dune morphologies in this section of the coast (i.e., coastline orientation,  
378 coarser sediment, nearshore bar system) (Figure 8 and 11).

379

### 380 **3.1.3 Upper beach and dune eroded volumes**

381 Erosion volume at the beach-dune interface was massive along the coast. The only part of the coast not  
382 affected by erosion is the extreme south (Cell 6.2), which even benefits from the sediment supply (Figure  
383 9). Along the coast, 71 % of the eroded volumes were taken from the dune front versus 29 % from the  
384 upper beach. However, differences are observable from north to south with a significant gradient  
385 illustrated by the linear regressions in Figure 9. We observe that the erosion in Cells 1, 2 and 3.1 was  
386 almost exclusively related to the dune retreat, and volume eroded from the upper beach represents less  
387 than 25 % (Figure 9). For example, in Cell 3.1, 88 % of the eroded volume at the beach-dune interface  
388 was taken to the dune. In Cells 3.2, 3.3, 3.4 and 3.5, the situation is more balanced and the eroded  
389 volumes at the dunes are comparable to the volumes eroded at the upper beach, showing that massive  
390 beach lowering and dune retreat are associated with this part of the coast. Total erosion at the beach-  
391 dune interface presents higher values along the coast until 3 165 103 m<sup>3</sup> is reached at Cell 3.3,  
392 representing an average erosion of approximately 166 m<sup>3</sup> per linear meter. In Cell 4, 96 % of the volume  
393 is eroded to the dune. In Cells 5.1 to 6.1 in Landes, erosion also mainly affects the dunes between 90 to  
394 62 %. Finally, the budget in Cell 6.2 is positive and accretions are mainly localized at the upper beach  
395 (85 %).

396



397

398 *Figure 9: Distribution of the eroded volume along the coast at the beach-dune interface between 2011*  
 399 *and 2014*

400 Even if we can consider that the entire coast was severely affected by beach erosion and dune retreat,  
 401 we found some substantial geographical differences that are also observable in the following period of  
 402 recovery in 2014-2017.

### 403 3.2. A progressive recovery between during the 2014-2017 period

#### 404 3.2.1 Incipient Foredune pattern

405 As well as for erosional patterns, almost all the coast was experiencing the recovery process during  
 406 2014-2017 (Figure 7 and 8). In 2017, 188 foredunes with a surface larger than 500 m<sup>2</sup> were detected  
 407 relative to the beach-dune state observed in 2014. The main characteristics of these foredunes are  
 408 between a 30 and 3360 m alongshore length and 4 to 77 m width.

409 Classes 1 and 2 represent 14.3 % and 33.0 % of the number of recovery marks detected, respectively,  
 410 and a total of 56.4 % and 30 % of the entire recovery area, respectively. Compared to erosional marks,  
 411 foredune patterns are generally larger in the alongshore direction. They are also thinner with an average  
 412 width of 18 m for Class 1 and 15 m for Class 2.

413 More local recovery marks are also observable in Classes 3 and 4, representing 27.1 and 25.5 % of the  
 414 total number of recovery marks, respectively. The widest foredune marks are observable in Cell 4 at the  
 415 spit of Cap Ferret, reaching more than 70 m. This massive accumulation of sand at the dune foot is  
 416 related to the hook ridge dynamic taking place at the Cap Ferret spit. Interestingly, comparing the sum  
 417 of the eroded area with the recovery area, only 9.0 % of the eroded area remained in the 2017 survey.

418 A geographic difference in the foredune pattern is clearly observable along the coast. Class 1, which  
 419 represents massive and longshore extended foredunes, is only observable in Landes (Cell 5.1, 5.2, and  
 420 5.3), except in the south of Gironde close to the Cap Ferret Spit. In Landes, classes 2 and 3 of the

421 foredunes are also observable, showing that foredune constitution is an important process in this part of  
422 the coast. Conversely, at the extreme north and south ends of the Aquitaine coast, incipient foredunes  
423 are poorly detectable or are only at a local scale (Class 3 and 4). Between the two, the center of the  
424 Gironde coast (3.3, 3.4 and 3.5) is mostly characterized by Class 2 and 3 foredune patterns. In Figure 6,  
425 the location of the Class 1 erosion form is almost opposite compared to recovery patterns. Locations for  
426 Classes 2 and 3 appear consistent, suggesting that foredunes can be promptly detected in previous dune  
427 scarp locations as observed by [Castelle et al., 2017](#). Finally, erosion and recovery in Class 4 do not  
428 appear to be connected.

429

### 430 **3.2.2 Cross shore beach-dune accretion**

431 Between 2014 and 2017, the progradation at the upper beach/foredune proxy was massive and generally  
432 observed all along the coast (Figure 11). The progradation was on average approximately 11 m and was  
433 greater than 20 m in many locations. The only part of the coast observing a retreat at this proxy are Cells  
434 2, 3.1 and 6.2. Notably, these cells were among the least affected by retreat during 2011-2014. For cells  
435 2 and 3.1 the poor progradation or stability seems to be related to the dynamic observed in 2011-2014  
436 to the specific nature and geology of this part of the coast. Evolution during the erosion and accretion  
437 phases at these elevation contours are limited due to paleo soil outcrops. For Cell 6.2, the reasons are  
438 less clear and are probably related to beach characteristics and the dominant longshore drift, which  
439 moves the sediment from south to north.

440 The dune foot location was also prograding at the Aquitaine coast scale, with a value of approximately  
441 2.1 m on average along the coast. Cells where the foredunes prograded the most are also those where  
442 the dune foot prograded the most (Cells 3.3, 3.5, 5.2 and 5.3). However, along the coast, evolutions at  
443 the dune foot can be notably variable with, for example, a mean progradation of approximately 4.6 m  
444 and 6.9 m in Cells 3.5 and 5.3, respectively, and a mean retreat of approximately 5.6 m and 0.9 m in  
445 Cells 2 and 7, respectively.

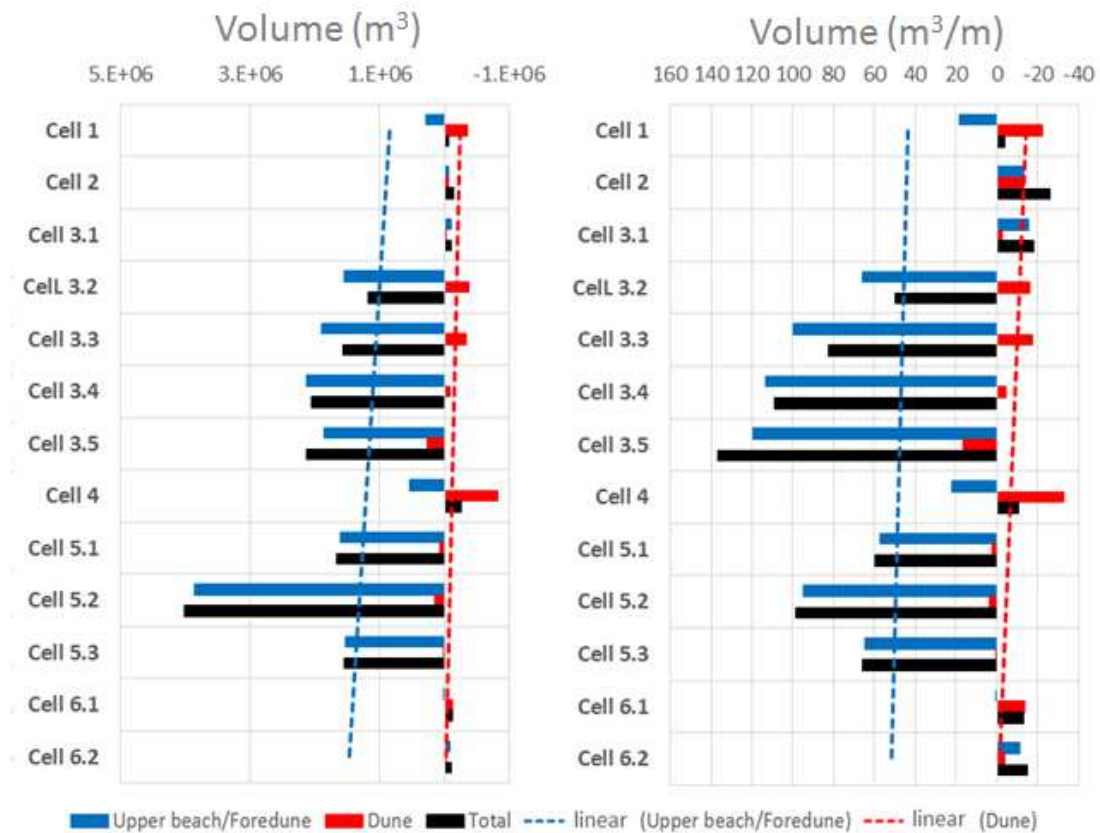
446 As expected, the dune front appears to be much more stable, mainly because recovery processes  
447 promoting dune front progradation generally take a longer time, such as several years to decades ([Hesp,  
448 2002](#)). However, some slight progressions of the dune front are observable in Landes (Cells 5.1 and 5.2)  
449 indicating a sand supply movement from the beach to the dune. This progradation can be significant,  
450 locally reaching 5 m to 8 m, and Cell 5.1 and Cell 5.2 are approximately 0.4 m on average. Conversely,  
451 the dune fronts in Gironde are mostly retreating (except locally in Cell 3.4). The retreat is on average  
452 greater than 2 m in Cell 1 and Cell 6, approximately 1.8 m in Cell 2 and approximately 1.3 m in Cells  
453 3.3, 3.4, and 3.5. This retreat is concomitant with a general accretion observable at the dune foot, which  
454 denotes an erosion sequence occurring during winters of the 2014-2017 period (discussed in section  
455 4.2).

456

### 457 **3.2.3 Volume recovery at the upper beach and dune interface**

458 Between 2014 and 2017, the gain in volume at the beach-dune interface was massive and was localized  
459 at 90 % of the upper beach. Dune erosion occurring during the winter of 2013-2014 are observable in  
460 Cells 1, 2, 3, 4 and 6, and accretion is mainly observable at the upper beach. Along Cells 3.5 and 5,  
461 accretion is massively observed on the beach (between 88 and 98 %) but also benefits to the dune front,  
462 which is consistent with the progradation showed by the dune front proxy (Figure 10). The volume  
463 stored in the automatically detected foredune pattern (Figure 6) represents only 13.5 % of the total  
464 recovered volume, which indicates that most of the sand volumes recovered in 2017 are localized on the  
465 upper beach and do not yet constitute established foredunes. This situation, which is prone to the

466 continuation of the recovery process is fragile, however, with the sand accumulated in the upper beach  
 467 being potentially remobilized during the following winters.



468  
 469 *Figure 10: Distribution of the recovered volume along the coast at the beach-dune interface between*  
 470 *2014 and 2017*

471 **3.3 Erosion and recovery balance and sediment budget**

472 **3.3.1 Planimetric evolution of the beach-dune interface (2011-2017)**

473 Previously, erosion and recovery were analyzed through two distinct periods; here, the difference in the  
 474 beach-dune state is regarded for the entire period (2011-2017), Figure 11.

475 Proxy results show that at the Upper dune/Foredune proxy, beaches have globally prograded since 2011  
 476 (+7.2 m). However, in northern (Cells 1 and 2) and central Gironde (Cell 3.2), no foredunes are  
 477 observable, or at least not as many are observable as in 2011. In the dune foot and the dune front, a quite  
 478 clear north-south gradient is observable (Figure 7).

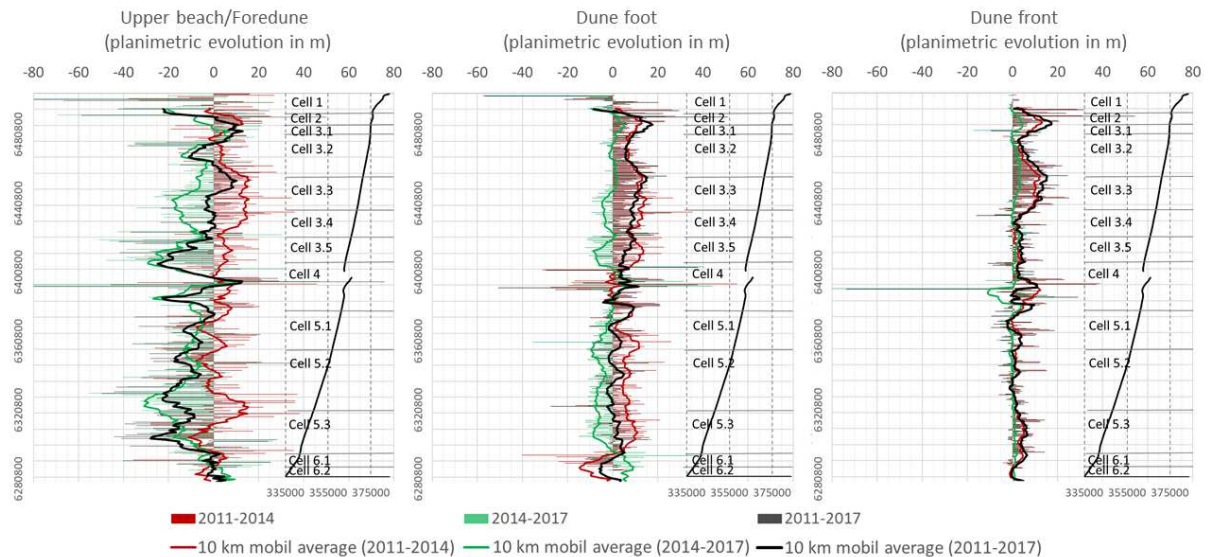
479 In Gironde, even if some recovery is noticeable after 2014, the sand supply and accumulation were not  
 480 sufficient at the dune foot and at the dune front to recover position before the 2013-2014 winter. In 2017,  
 481 dune fronts still present a retreat between 2 m and 10 m compared to 2011.

482 Cell 4, being at the direct proximity of the tidal inlet of Arcachon lagoon, is submitted to a specific  
 483 evolution process and some local instability of the coastline can trigger a massive retreat or progradation  
 484 at the annual time scale. However, the trend indicates substantial erosion on average during the 2011-  
 485 2017 period.

486 In Landes (Cell 5), the situation is different. With a few exceptions along the coast, the upper  
 487 beach/foredune was significantly prograding at approximately 11.7 m on average, and the dune foot as

488 well as dune front appears to be quite stable between 2011 and 2017 (Figure 11). Even if erosion marks  
 489 were observable in 2014, a substantial sand supply compensated for losses in many locations. Cell 5.2  
 490 has an almost stable balance with retreats between 2011 and 2017 of only approximately 0.8 and 0.7 for  
 491 the dune foot and the dune front, respectively. In Cell 5.3, the balance is also nearly stable at the dune  
 492 foot (-0.5 m) but is clearly negative for the dune front (-4.1 m).

493 At the extreme south of Landes (Cells 6.1 and 6.2), the situation is contrasted; Cell 6.1 presents a notably  
 494 negative balance at the dune front (-7.1 m) and Cell 6.2 is positive (+1 m).



495  
 496 *Figure 11: Planimetric differences between 2011 and 2017 at the foredune, the dune foot and the front*  
 497 *dune proxies. The black line on the right-sides of each panel represent (plan view of the shoreline).*

### 498 3.3.2 Sedimentary budget

499 Consistent with the other analyses, we observe that beach and dune systems have dramatically lost sand  
 500 between 2011 and 2014, mainly because of the extremely active 2013-2014 winter (Figure 5). More  
 501 than  $15\,500 \times 10^3 \text{ m}^3$  have left the beach-dune interface during this period, which represents an average  
 502 loss of  $66 \text{ m}^3$  per linear meter. The gains during the following period (2014-2017) are also massive and  
 503 concern almost all the coast. Apart from Cell 5.1 directly downstream of the Arcachon inlet, the parts  
 504 of the coast still presenting erosion were the extreme north and south. In total, the accretion was larger  
 505 than  $13\,500 \times 10^3 \text{ m}^3$  with an average gain of  $57 \text{ m}^3$  per linear meter.

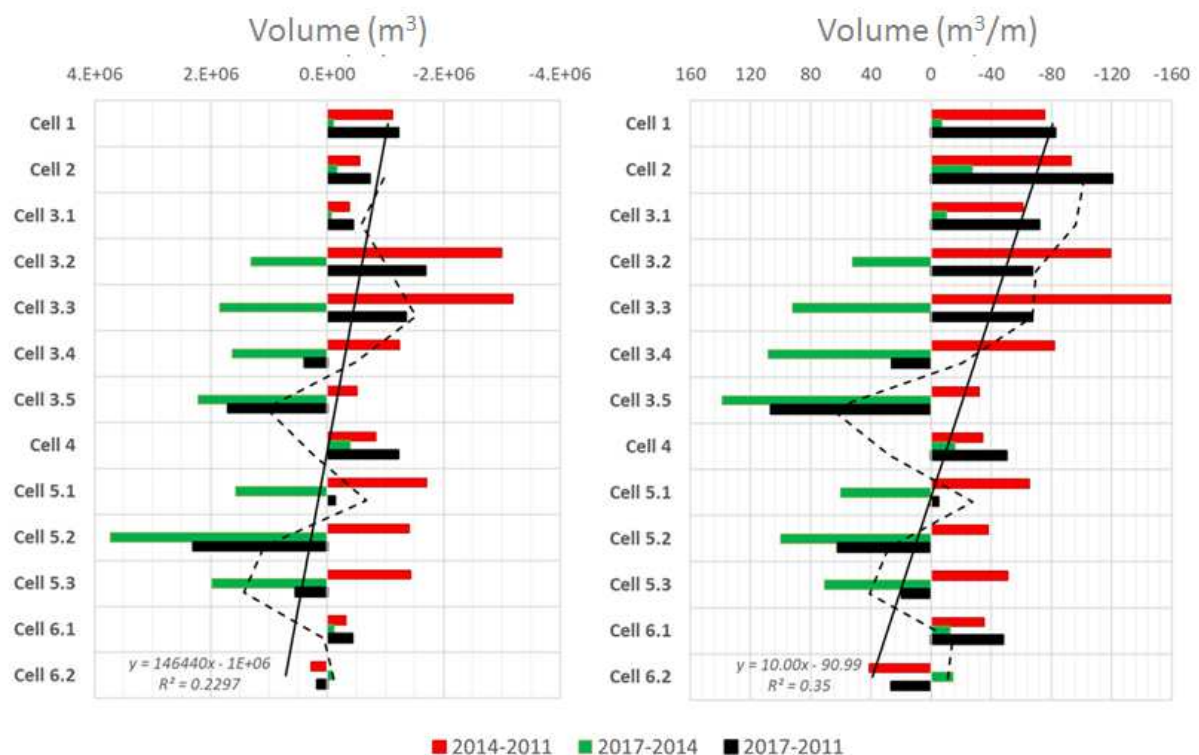
506 Considering the total budget between the two periods, 86.5 % of the sand eroded at the beach-dune  
 507 interface in 2014 returned to the beach-dune interface in 2017. Interestingly, we observe that the  
 508 sediment that moved to the subaerial system follows the north-south dominant longshore drift (Figure  
 509 11). If we consider sub-Cells 3.1 to 3.5 and 5.1 to 5.3, we observe that sand volumes have migrated  
 510 downstream. This process was generally characterized by a greater amount arriving at the contiguous  
 511 downstream subcell (Figure 10).

512 If Cell 1 is excluded from the budget due to its singular characteristics and dynamics at the scale of the  
 513 Aquitaine coast (divergent longshore drift direction, source of sediment, the urbanization of the coast,  
 514 dune structuration, and presence of paleo soil outcrops), then only 7 % of the eroded volume has not  
 515 returned to the beach-dune interface.

516 In the center of Gironde (Cells 3.2, 3.3, 3.4 and 3.5), a massive sand supply during 2014-2017 is partly  
 517 compensating for sediment losses that occurred in 2014 (Figure 12). However, the balance is negative  
 518 for Cells 3.2 and 3.3, whereas it appears positive in Cells 3.4 and 3.5 even if the dune front has strongly  
 519 retreated in some locations. This can be explained by the eroded volumes in 2014 following a north-  
 520 south gradient (Figure 9), thus affecting Cells 3.2 and 3.3 more substantially than Cells 3.4 and 3.5.  
 521 Furthermore, at the beginning of the north-south oriented longshore drift (Cells 2 and 3.1), sediments  
 522 are rarely available due to no significant natural sand supply source in the system from the north and  
 523 limited stocks directly on the beach (paleo soil outcrop). The only significant source of sediment in this  
 524 part of the coast is the eroded sand from the dune fronts.

525 The downstream subcells 3.4 and 3.5 benefit from a massive sediment supply, but even if the sediments  
 526 massively returned to the beach-dune interface, the dune fronts have not clearly prograded and are still  
 527 in their positions reached after the 2013-2014 winter. The sand recovered in this part of the coast is  
 528 mainly stored in the upper beach and in some incipient foredunes. The recovery process should be  
 529 considered as partial because in this position sediments can be more easily removed during storm  
 530 energetic events.

531 The Landes coast has massively recovered sand, benefiting many dune front locations. For example, in  
 532 Cell 5.2 the balance between 2011 and 2017 is notably positive with an average gain of approximately  
 533 62 m<sup>3</sup> per linear meter (Figure 12). The situation is more contrasted in southern Landes, with Cell 6.1  
 534 having substantial erosion during the two consecutive periods and Cell 6.2 surprisingly showing erosion  
 535 during 2014-2017, despite undergoing gains during 2011-2014. This opposite dynamic can be explained  
 536 by the specific orientation of the coast. Longshore drift in this part of the coast can be unstable depending  
 537 on the incoming wave orientation, particularly during storm erosive events, and can explain the  
 538 contrasted evolution observed in 2014. Conversely, the results in 2017 suggest that a south-north  
 539 longshore drift is dominating, damaging Cell 6.2.



540

541 *Figure 12: Sediment budget along the coast at the beach-dune interface between 2011 and 2017. Left*  
542 *panel is total  $m^3$  and right panel is in  $m^3/m$ . The black dashed line is a mobile average curve of 2011-*  
543 *2017 evolutions*

### 544 3.3.3 Pluriannual trends

545 The previous treatment has shown that the beach-dune interface evolution presents highly variable  
546 trends along the coast during 2011-2014 as well as 2014-2017.

547 Globally, the situation is at a progressive reconstruction of the sand stocks from the nearshore to the  
548 beach dune system. However, some cells are following other trajectories. To illustrate those various  
549 trajectories at the decadal scale, the analysis during the 2011-2017 period is completed by d-GPS data  
550 since 2006. Additionally, pluridecadal trends based on historical photography analysis since 1985 and  
551 DSAS treatment (Bernon et al., 2016) are applied to the last decade's evolutions. To be consistent, the  
552 dune foot location (Df, cf. section 2.1) is considered for the three datasets. For the illustration, the long-  
553 term trend goes back to 1985, but it is shown with 2006 as a reference starting point. The rates of erosion  
554 determined at pluriannual (including an extremely energetic winter), decadal and pluridecadal scales are  
555 then compared in Table 3 and Figure 13.

556

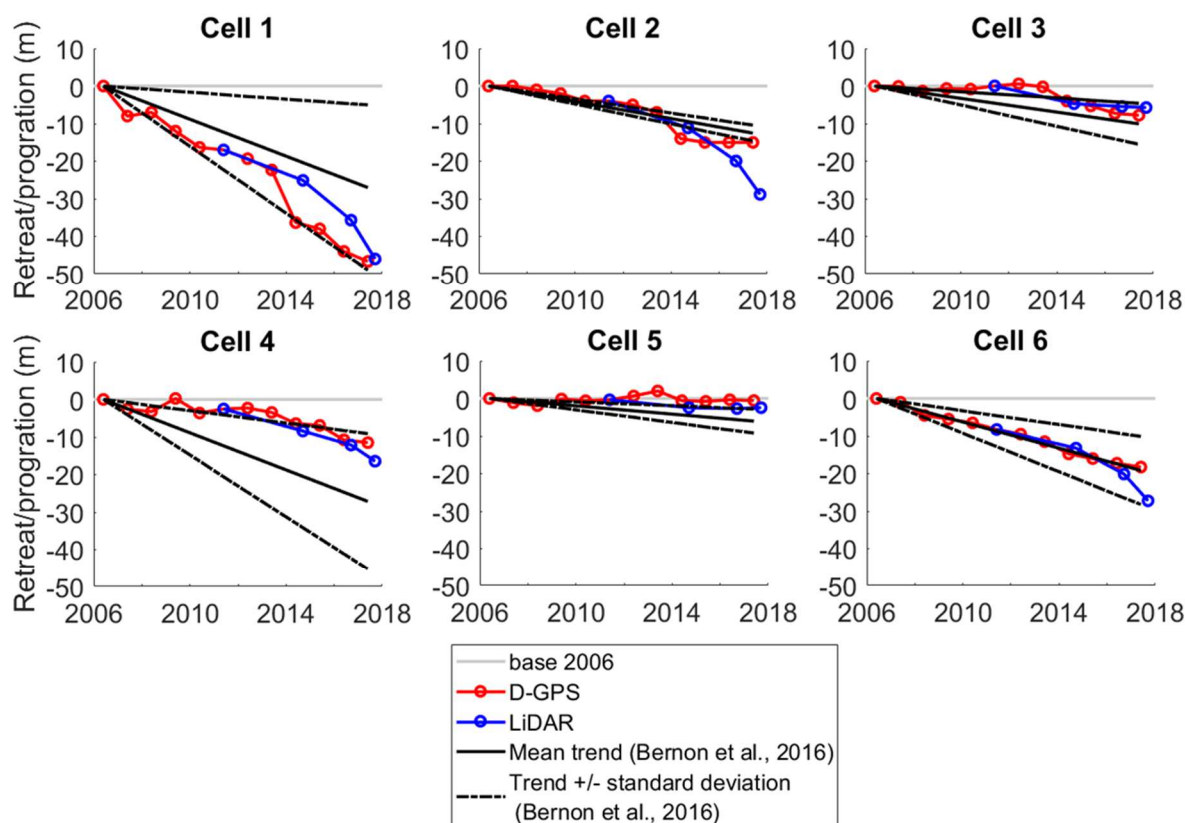
557 *Table 3: Rate of coastline evolution along the Aquitaine coast at pluri-annual, decadal and pluri-*  
558 *decadal time scales*

559

560 We generally observe a quite strong consistency between the three methods and the three periods (Figure  
561 13). Apart from Cell 1, where local erosions are massive and are partly influenced by coastal structures  
562 and Cell 2, where the discrepancy between LiDAR and d-GPS measurement is basically due to the  
563 number of surveyed profiles (only one), results obtained from the d-GPS network and the LiDAR  
564 analysis present similar rates of evolution for each cell. This suggests that parts of Cells 1 and 2 were  
565 more contrasted due to local specificities; the OCA d-GPS network gives valuable and representative  
566 information about the trend of evolution for each sedimentary cell.

567 For the rate of erosion, we observe that during the last decade, the dune retreat trends in Cells 1 and 2  
568 are notably faster than expected in pluridecadal analysis (Bernon et al., 2016). D-GPS and LiDAR data  
569 show a fast and continuous erosion close to mean pluridecadal trend and a standard deviation during the  
570 last decade. In Cell 2, rates are slower, but the tendency during the last decade is higher than the  
571 pluridecadal trend. Furthermore, LiDAR data show even faster rates during the final years due to no  
572 significant recovery occurring since 2014.

573 Interestingly, for Cells 3, 4, and 5, the very similar rates obtained by d-GPS and LiDAR show that the  
574 erosion in the last decade was slower than the rhythm observed since 1985, which is generally near a  
575 trend of less than a standard deviation. In Cell 6, all the trends are consistent and show that Cell 6 and  
576 Cell 2 present similar dynamics of erosion during the last decade and are the second most affected  
577 sections along the coast after Cell 1.



578

579 *Figure 13: Comparison of erosion trajectories for sedimentary Cells at interannual, decadal and*  
 580 *pluridecadal scales*

581

## 582 4 Discussion

### 583 4.1 Beach-dune evolutions at an interannual resolution

584 First, topographic measurements such as LiDAR surveys are snapshots of beach states. That implies that  
 585 the interannual evolution of the beach-dune integrates many successive changes and should be  
 586 interpreted with caution. This is especially the case when an analysis of pluriannual evolutions is done,  
 587 whereas LiDAR surveys occur at various seasons of the year. In these conditions, differential analyses  
 588 can be biased considering, for example, pre- and post-winter beach states.

589 In our study, LiDAR surveys occurred mostly during the same period of the year, after the summer  
 590 season and just before the beginning of winter. The only discordant survey was made in 2011 before  
 591 summer. In other words, the comparison between 2011 and 2014 includes that beach-dune systems in  
 592 2011 are marked by the winter state of the profiles (i.e., low intertidal beach and potentially eroded  
 593 foredunes).

594 Conversely, the 2014 survey was made after summer, which means this campaign integrates the seasonal  
 595 summer evolution just after the 2013-2014 winter storms. [Castelle et al., 2017](#) illustrated that some  
 596 locations along the coast, similar to those in Truc Vert beach, have experienced a noticeable recovery  
 597 during the 2014 summer. This recovery is characterized by the installation of an incipient foredune at  
 598 the contact of the dune foot, with some pioneer vegetation installation. However, it takes one more year  
 599 (Autumn 2015) to observe the installation of a substantial foredune. This local observation is consistent  
 600 with our analysis, which shows that at the Upper beach/Foredune altimetric proxy (Figure 8 and 11)  
 601 some parts of the coast (South Gironde and Landes) have already recovered a configuration nearly

602 comparable to 2011 in Autumn 2014. However, in sections of the coast that were massively eroded  
603 during the 2013-2014 winter (like north and center Gironde), the beach-dune interface appears highly  
604 impacted even after the summer season. Furthermore, the foredune pattern detection indicates only a  
605 small number of foredunes between the 2011 and 2014 surveys. Those incipient foredunes are only  
606 detected at the extreme north of Cell 1 (banc Saint Nicolas), locally at the south of the Arcachon inlet  
607 and along the Landes coast (Cells 5.1, 5.2, 5.3). This indicates that recovery surely occurred at the upper  
608 beach, whereas foredunes were still low or nonexistent along the coast after the 2014 summer.

609 Considering that the urbanized coastline in the sandy Aquitaine coast is very local (representing less  
610 than 10 % of the total coastline), the analysis of erosion processes taking place directly around the  
611 urbanized coastline is not integrated in this study. However, after the 2013-2014 winter and at an annual  
612 frequency, beach management actions, including beach nourishment, sand removal upstream from the  
613 drift, beach reshaping or dune stabilization occur along the coast. These actions take place along or near  
614 the urbanized coastline and are at volumes of generally approximately  $50 \times 10^3 \text{ m}^3$  or less. The supply  
615 or modification of the sediment transit along the coast are expected to have impacts only at a local scale  
616 and have no significant effect on the analysis at the regional scale. This observation must be balanced  
617 concerning Cell 6, where the results can be influenced by the large Capbreton groin and the annual  
618 artificial bypass action.

#### 619 **4.2 Sediment availability and recovery process**

620 The beach profile evolutions and the cells and subcells' sediment budgets analyzed previously suggest  
621 that during the successive storms of the 2013-2014 winter, most of the sediments eroded on the beach-  
622 dune interface were moved to the subtidal beach by cross-shore dominant processes ([Castelle et al., 2015](#)).  
623 Unfortunately, no bathymetric data are available to support this hypothesis and teledetection-  
624 based analysis of the bar configuration or estimating the sediment volume of the nearshore area are not  
625 in the scope of this study. However, because (i) currently, no significant amount sand is supplied by the  
626 rivers (Gironde, Leyre or the small rivers of the Landes); and (ii) in many parts of the coast, beach have  
627 quickly and continuously recovered sediment (in the first month following the winter and over several  
628 years). Therefore, most parts of the eroded sediment have likely remained within the nearshore system,  
629 being stored on the subtidal beaches.

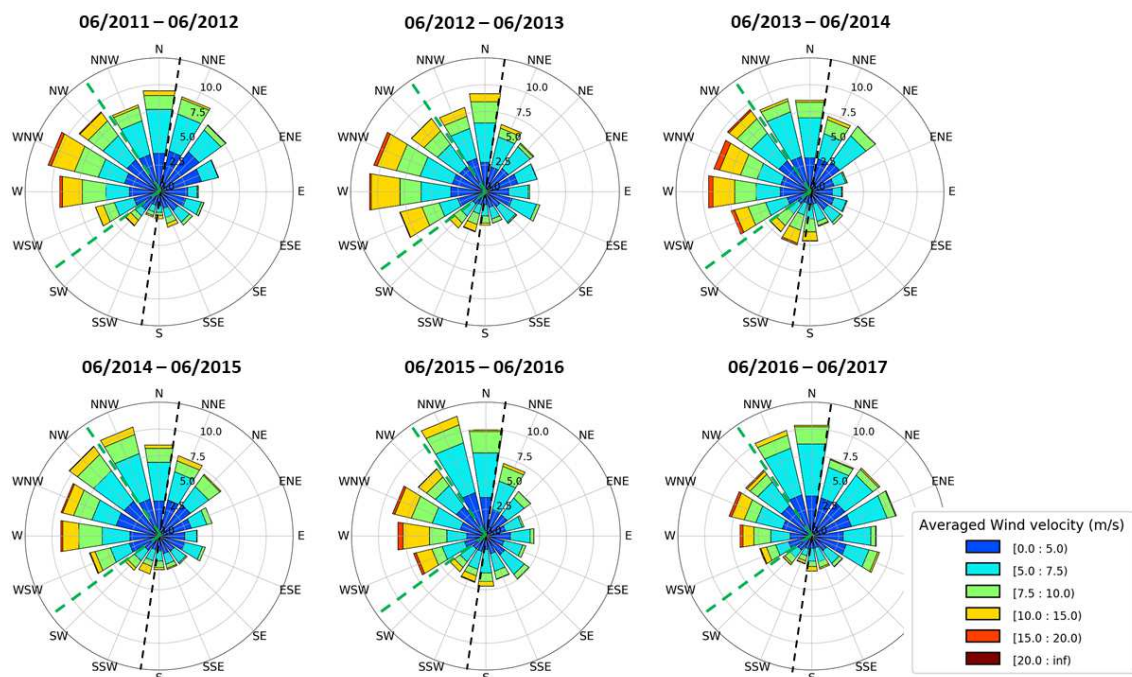
630 Previous estimation of chronic loss related to coastline retreat in Gironde coast where approximate at  
631 between  $-15 \text{ m}^3/\text{m}/\text{yr}$  and  $-20 \text{ m}^3/\text{m}/\text{yr}$  ([Aubié and Tastet, 2000](#)). Our results show significantly weaker  
632 average loss in Gironde  $-6.7 \text{ m}^3/\text{m}/\text{yr}$  on the 2011-2017 period and finally stable to positive sediment  
633 budget in Landes with gain about  $1.6 \text{ m}^3/\text{m}/\text{yr}$ . The sediment budget for all the coast between 2011 and  
634 2017 shows a deficit of  $2\,000 \times 10^3 \text{ m}^3$ . It is uncertain that these sediments can be mobilized and return  
635 to the beach-dune interface. If we refer to the estimations of [Aubié and Tastet \(2000\)](#), 600 to 900  $\text{m}^3/\text{yr}$   
636 would be likely to leave the system by migrating offshore in response to sea level rise. They suggest  
637 that this amount of sediment would be deposited offshore beyond the depth of closure. Considering that  
638 response of sea level rise should be similar along the all Aquitaine coast these estimations look  
639 overestimated compared to the results obtained. Our results are more in line with findings of [Bellessort  
640 and Migniot \(1987\)](#) which found loss related to sea level rise to between 200 and 300  $\text{m}^3/\text{yr}$ . However,  
641 if the effects of sea-level rise are likely to be responsible for a part of this sediment migration, the  
642 dynamics of the currents associated to the extreme storms of winter 2013-2014 also played a role in this  
643 offshore migrations.

644 Between 2014-2017, an overall pluriannual tendency of recovery is observed. Winters during this period  
645 were variably intense but are generally low to moderately energetic. During only a few events, TWL  
646 barely reached 5 m/NGF (Figure 5), thereby preventing a major part of the coast from experiencing  
647 incipient foredune dismantlement. The dune scarp and associate erosion detected during this period

648 indicate that the coast was affected in a significant number of locations (52 in total). However, the length  
 649 of those eroded areas were mostly lower than 400 m (Classes 3 and 4), and the only part of the coast  
 650 significantly affected during the winters of the 2014–2017 period was northern Gironde (Cell 1 and 2,  
 651 3.2), where two erosion scarps of Class 1 were detected and the dune front has retreated between 5 and  
 652 10 m.

653 More generally along the coast, benefiting from moderately energetic winters and available sediment in  
 654 the nearshore area, sand has massively recolonized the upper beach, being driven by a mix of marine  
 655 and aeolian driven processes. The parts of each dynamic at this spatial and temporal scale benefiting at  
 656 the upper beach appear unclear (4 m/NGF contour). However, at contours higher than 5 m/NGF (and  
 657 thus at the dune foot proxy), sediments are more obviously supplied by aeolian processes. Consistently,  
 658 automatically detected foredunes that are in contact with the dune foot generally exhibit more longshore  
 659 extended dimensions than erosion patterns as related to zonal and longshore homogenous aeolian  
 660 processes.

661 Analysis of wind sector distributions indicate that the 2014 – 2017 period was favorable to foredune  
 662 accretion relative to general wind characteristics (Figure 2) and to the previous period (Figure 14). An  
 663 average 10 m wind distribution at the center of the coast (Cell 4), which is quite similar to along the  
 664 coast, is presented (Figure 14). The most constructive winds (NNW to N > 5 m.s<sup>-1</sup>) which represents in  
 665 annual average around 10 % of the total winds are overrepresented during the period. They exceed 13  
 666 % between 06/2015-06/2016 and 15 % between 06/2016-06/2017. The recovery sequence was thus both  
 667 allowed by moderately energetic winters and rather favorable winds during springs and summers.



668  
 669 *Figure 14: Annual wind characteristics at the Cell 4 during the studied period. Dashed black lines*  
 670 *represent the coastline orientation at each sedimentary cell and the green dotted line delimits a more*  
 671 *favorable wind orientation for foredune accretion (from north and southwest)*

672

### 673 4.3 Beach-dune recovery stages

674 Erosion patterns at the beach-dune interface are caused by hydrodynamic conditions (water level and  
 675 wave characteristics) and their dimensions depend on the preexistent nearshore and intertidal beach

676 morphology. Conversely, foredune installation is mainly an aeolian process that on relatively straight  
677 coasts is likely to be more homogenous in the alongshore direction. The recovery process related to the  
678 foredune installation, dune foot rise and sand migration to the dune front, is much slower than the erosion  
679 process, generally taking several years.

680 If the coast has mainly recovered since 2014, then this trend is not homogenous and follows a variable  
681 rate depending on the cells. This leads to variable morphological evolutions observed along the coast.  
682 These evolutions of the beach-dune profile can be synthetized as follows (Figure 15):

683 **Stage 1, “massive storm erosion”**, is the configuration observed directly after a winter that has caused  
684 massive beach erosion and dune front retreat. This situation can be extended in time or be accentuated  
685 when the beach is affected by a chronical erosion. Along the Aquitaine coast, this case is observable  
686 mainly in Cells 1, 2 and 3.1, where interannual recovery processes are generally not observable and  
687 beaches are permanently characterized by eroded profiles.

688 **Stage 2, “upper beach recovery”**, represents the recovery of the upper part of the beach. This situation  
689 can be observed a few months after the erosive events in the case of sediment availability, calm marine  
690 conditions and favorable winds (moderate intensity northward winds in the Aquitaine coast). After  
691 several years, this situation is characteristic of a weak potential for recovery of the system due to low  
692 sediment availability and regular erosion even during moderate storms. This situation is locally  
693 observable in some parts of Cells 2, 3.1 and northern Cell 3.2.

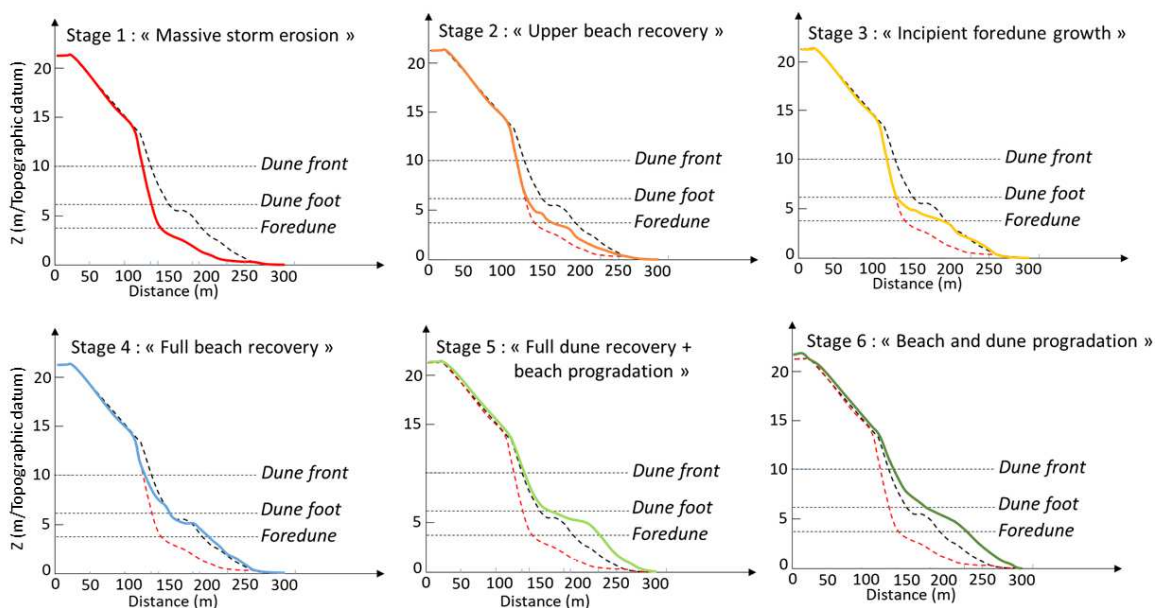
694 **Stage 3, “incipient foredune growth”**, shows the constitution of an incipient foredune that can to some  
695 extent recover the planimetric position of the beach profile before the erosive sequence. [Castelle et al.,  
696 2017](#), based on regular d-GPS surveys, showed that this situation was observable a year and a half after  
697 winter 2013-2014 in the south of Gironde (Cell 3.5). After 3 years, Cells 3.2 and 3.3 present this kind  
698 of profile, illustrating a slower recovery process at the center of Gironde, which is probably due to a  
699 lack of sediment available in the subtidal and intertidal beaches and a southward migration of the  
700 sediment eroded during the 2013-2014 winter.

701 **Stage 4, “full beach recovery”**, is characteristic of recovering beaches where sediments are available  
702 on the subtidal and intertidal beaches. Aeolian processes are actively moving sand to the dune foot and  
703 pioneer vegetation is installed at the foredune, thus facilitating sand deposits. The slope break  
704 characterizing the dune foot tends to be smoothed and raised. This configuration after three years of  
705 relatively calm storm activity globally follows the rate evocated by several authors (e.g., [Ollerhead et  
706 al., 2013](#), [Houser et al., 2015](#)), who suggest that massive erosion on dunes whose height is greater than  
707 10 m takes several decades to fully recover considering the shape, position and volume. Even if the  
708 situation is prone to promote an acceleration of the sand accumulation thanks to the installation and the  
709 development of the back shore vegetation in this recovery step ([Hesp 2002](#); [Houser et al. 2015](#)), the  
710 recovery process remains fragile. Energetic storms can destabilize the recovery process, causing new  
711 beach scarps and affecting the vegetation. This kind of profile is observable in Cells 3.4 and 3.5 and  
712 more commonly in Cells 5.1, 5.2 and 5.3.

713 **Stage 5, “beach-dune recovery”**, is observable mainly in the Landes coast, where after the 2013-2014  
714 winter, the beach digging was significantly less important compared to the Gironde coast and where no  
715 major erosion was observed at the dune front. In this case, sediment returning to the beach and the  
716 backshore benefits the dune, generating a continuous sand ramp from the dune foot to the dune front  
717 (Figure 15). The dune foot is still elevating, and the slope break is not clearly detectable. Sand is then  
718 accumulated at the dune front. With a massive sediment supply, a new incipient foredune can also  
719 appear. This kind of evolution is observable mostly in the Landes coast (particularly Cells 5.1 and 5.2).

720 **Stage 6, “Beach-dune progradation”**, a few profiles presenting dune front progradation and sand  
 721 accumulation at the dune crest are observable in Landes. They are mainly localized where erosive  
 722 impacts during the winter 2013-2014 were very low or limited at the intertidal beach. They present a  
 723 progressive accumulation of sand on the dune front since 2011 leading to a reduction of the dune front  
 724 slope and an elevation of the dune crest. Dune crest evolution were generally important between 2011-  
 725 2014 (approximately 2 m) and then a more progressive accretion occurred between 2014-2017. These  
 726 differences in elevation rates suggest, in accordance with Hesp, 2002, that dune crest accretion for steep  
 727 and high dunes (approximately 20 m) is mostly generated by strong winds. This can be an explanation  
 728 of the relatively few changes of the dune crest during 2014-2017 in comparison with 2011-2014 mainly  
 729 because of low energy winters.

730



731

732 *Figure 15: Schematic recovery stages observed along the Aquitaine coast. The black and the red*  
 733 *dashed lines indicate the pre-/post-erosive sequence profiles respectively*

734 The presented conceptual evolution based on the observations of cross-shore profile behaviors along the  
 735 coast is mainly valuable for sandy open coasts. The dynamic at Cell 1 is characterized by chronic erosion  
 736 and a nearshore environment constituted by submarine rocky platforms and paleo soil outcrops at the  
 737 dune foot. These singular conditions along the Aquitaine coast prevent us from including this part of the  
 738 coast in the previous classification. At Cell 4 and mostly at the south of the Arcachon inlet, the direct  
 739 proximity of the tidal inlet and the sand banks generate a complex and local evolution. Foredunes and  
 740 dunes are much more unstable, generating a local progradation or retreat at a short time scale as observed  
 741 in Figure 11. Finally, the beach-dune morphologies and behavior at the south of Landes (Cell 6) are  
 742 different, which is mainly due to coarser sediment. Beach slopes are steeper, exhibiting successive  
 743 berms, and dunes are lower. Aeolian dynamics are comparatively reduced due to coarser sediments and  
 744 the limited width of the potential dry beach.

745

746

## 747 5. Conclusion

748 A method coupling a GIS automatic detection of dune scarps and incipient foredunes, a cross-shore  
749 morphometric indicators analysis and a sediment budget was applied to analyze erosion and recovery  
750 processes at a regional scale. The three approaches appear complementary and give consistent results.

751 Between 2011 and 2014, particularly after 2013-2014, which was the most energetic winter since 1948,  
752 erosion marks were generalized along the coast and are qualitatively linked with typical nearshore bar  
753 configurations, intertidal beach heights and the beach width. Erosion marks were classified in several  
754 classes, including a highly homogenous longshore erosion band (>1 km length), mega cusps of variable  
755 alongshore lengths (from 200 to 800 m) and local erosion marks. A clear north to south gradient was  
756 observed for eroded surfaces, volume losses and dune front retreats. The opposite recovery processes,  
757 which have taken place since 2014, are generally more marked from south to north, leading to a clearly  
758 contrasted trajectory in term of coastline evolutions.

759 In Gironde, the northern cells present chronic erosion between 2011 and 2017 related to massive erosion  
760 characterized by a longshore uniform mark, and no recovery is observable during the 2014-2017. In  
761 central and south Gironde, the major parts of the coast have benefitted from massive recovery between  
762 2014 and 2017. However, locally, profiles have continued to retreat during the winters of 2014-2017.  
763 Dune fronts have not significantly prograded since the massive erosion of winter 2013-2014.

764 The coast of Landes shows a noticeable rhythm of progradation at the upper beach/foredune, dune foot  
765 and dune front proxies, benefiting from a smaller impact during the 2013-2014 winter and abundant  
766 sand being available. Beaches of this part of the coast appear to be stable or in accretion, leading to dune  
767 front progradation in some locations since 2011.

768 Three and a half years after the 2013-2014 winter, the sediment budgets at a regional scale suggest that  
769 the major part (86.5 %) of the sand taken from the beach by cross-shore processes have moved back to  
770 the beach-dune interface. However, massive sand volume has returned, moving southward following  
771 the dominant longshore drift and accentuating the sediment deficit in the northern cell of the coast (Cell  
772 1, 2, 3.1 and 3.2). Many questions remain concerning the cross-shore and the longshore migration of the  
773 sand during the winter of 2013-2014 and during the observed recovery sequence in 2014-2017. This  
774 analysis was based only on topographic data and must be further investigated and supported by  
775 complementary studies dedicated to analyzing the behavior of the subtidal beaches during this period.

776 Pluridecadal trends of coastal evolution are consistent with LiDAR and d-GPS analyses covering the recent  
777 period. Comparison with ortho-photography from 1985 suggests no significant acceleration of the  
778 erosion rate along the coast during last decade even when the effects of the 2013-2014 winter are  
779 considered.

780 Taking into account that dune front recovery (shape and position) can take decades with an adequate  
781 sediment supply, the progressive recovery tendency observable at the beach-dune interface is fragile,  
782 particularly in the case of central and south Gironde, where sediments are mainly stocked between the  
783 upper beach and the dune foot and are potentially removable by storm marine processes. Even if the  
784 sediment budget from the upper beach to the dune is negative between 2011 and 2017 ( $\sim 2\,000 \times 10^3$   
785  $\text{m}^3$ ) along the 230 km of the Aquitaine coast, the coastal system of the Aquitaine coast still has a high  
786 possibility of recovering in a few years. The massive sediment loss observed after the great winter of  
787 2013-2014 at the beach-dune interface was recovered in most parts of the coast. After several years of  
788 relatively moderately energetic conditions and favorable winds, the upper beach has been recolonized,  
789 constituting foredunes and even generating dune front progradation. These results illustrate the  
790 relevance of the policies in place in the Aquitaine coast, based on soft sediment management and  
791 preventing coastline fixation and massive structures as much as possible along the coast. Sustainable

792 sediment management must be organized at a regional scale by taking into account potential interannual  
793 massive cross-shore and alongshore dynamics.

794

#### 795 **Acknowledgments:**

796 The authors are grateful to the Observatoire de la Côte Aquitaine (OCA) for providing data resources in  
797 partnership with the ONF and the IGN for LiDAR Data. All cofunders of the OCA project are thanked,  
798 namely, the European Union via the FEDER fund, the SGAR, the Région Nouvelle-Aquitaine, and the  
799 department of Gironde, Landes and Pyrénées-Atlantiques. The authors want to gratefully acknowledge  
800 the anonymous reviewers for their constructive criticism and insightful comments that greatly improved  
801 the manuscript.

802

#### 803 **Bibliography :**

804 Aleman, N., Robin, N., Certain, R., Anthony, E. J., & Barusseau, J. P. (2015). Longshore variability of  
805 beach states and bar types in a microtidal, storm-influenced, low-energy  
806 environment. *Geomorphology*, 241, 175-191.

807 Almeida L.P. , Vousdoukas M.V. , Ferreira Ó. , Rodrigues B.A, Matias A. (2012), Thresholds for  
808 storm impacts on an exposed sandy coastal area in southern Portugal *Geomorphology*, 143–144 pp. 3-  
809 12, 10.1016/j.geomorph.2011.04.047

810 Andrews, B., Gares, P.A., Colby, J.D., (2002). Techniques for GIS modeling of coastal dunes.  
811 *Geomorphology*, 48(1-3), 269-287.

812 Angnuureng, D. B., Almar, R., Senechal, N., Castelle, B., Addo, K. A., Marieu, V., & Ranasinghe, R.  
813 (2017). Shoreline resilience to individual storms and storm clusters on a meso-macrotidal barred  
814 beach. *Geomorphology*, 290, 265-276.

815 Aubie, S. and Tastet, J.-P., 2000. Coastal erosion, processes and rates: an historical study of the Gironde  
816 coastline, southwestern France. *Journal of Coastal Research*, 16(3), 756-767. West Palm Beach  
817 (Florida), ISSN 0749-0208.

818 Bellesort, B. and Migniot, C., 1987. Catalogue sédimentologie des cotes Françaises. Partie C: de la  
819 Gironde à la frontière espagnole, Rapport LCHF-STC, Collection de la Direction des Etudes et  
820 Recherches d'Electricité de France, Eyrolles (ed.), pp. 371-552.

821 Bender, C. J., & Dean, R. G. (2003). Wave field modification by bathymetric anomalies and resulting  
822 shoreline changes: a review with recent results. *Coastal Engineering*, 49(1-2), 125-153.

823 Bernon N., Mallet C., Belon, R., avec la collaboration de Hoareau A., Bulteau T. et Garnier C. (2016) -  
824 Caractérisation de l'aléa recul du trait de côte sur le littoral de la côte aquitaine aux horizons 2025 et  
825 2050. Rapport final. BRGM/RP-66277-FR, 99 p., 48 Ill., 16 tab., 2 ann., 1 CD.

826 Biauxque M And Senechal N. (2018). Storms impacts on a sandy beach including seasonal recovery:  
827 alongshore variability and management influences. *Revue Paralia*, Vol. 11, pp n02.1–n02.16. DOI:  
828 <https://doi.org/10.5150/revue-paralia.2018.n02>

829 Boak, E. H., & Turner, I. L. (2005). Shoreline definition and detection: a review. *Journal of coastal  
830 research*, 688-703.

831 Brenner, O. T., Lentz, E. E., Hapke, C. J., Henderson, R. E., Wilson, K. E., & Nelson, T. R. (2018).  
832 Characterizing storm response and recovery using the beach change envelope: Fire Island, New  
833 York. *Geomorphology*, 300, 189-202.

834 Brock, J. C., & Purkis, S. J. (2009). The emerging role of lidar remote sensing in coastal research and  
835 resource management. *Journal of Coastal Research*, 1-5.

836 Bulteau T., Mugica J., Mallet C., Garnier C., Rosebery D. Maugard F., Nicolae Lerma A., Nahon A.  
837 and Millescamps B. (2014). Evaluation de l'impact des tempêtes de l'hiver 2013-2014 sur la  
838 morphologie de la côte Aquitaine. Rapport final BRGM/RP-63797-FR, 68p.

839 Bulteau T., Nicolae Lerma A., and Mugica J. (2016). Caractérisation de l'exposition du littoral Aquitain  
840 à l'aléa submersion marine. Rapport final. BRGM/RP-63802-FR

841 Bulteau, T., Paris, F., Nicolae Lerma, A., Muller, H. (2019) - Le réseau tempêtes de l'Observatoire de  
842 la Côte Aquitaine. Rapport final. BRGM/RP-67418-FR, 72 p

843

844 Burvingt, O., Masselink, G., Russell, P., & Scott, T. (2017). Classification of beach response to extreme  
845 storms. *Geomorphology*, 295, 722-737.

846 Castelle, B., Bonneton P., Dupuis H., Sénéchal N. (2007). Double bar beach dynamics on the high-  
847 energy meso-macrotidal French Aquitanian coast, *Marine Geology*, 254 216-223.

848 Castelle, B., Marieu, V., Bujan, S., Splinter, K. D., Robinet, A., Sénéchal, N., & Ferreira, S. (2015).  
849 Impact of the winter 2013–2014 series of severe Western Europe storms on a double-barred sandy coast:  
850 Beach and dune erosion and megacusp embayments. *Geomorphology*, 238, 135-148.

851 Castelle, B., Bujan, S., Ferreira, S., & Dodet, G. (2017). Foredune morphological changes and beach  
852 recovery from the extreme 2013/2014 winter at a high-energy sandy coast. *Marine Geology*, 385, 41-  
853 55.

854 Castelle, B., Guillot, B., Marieu, V., Chaumillon, E., Hanquiez, V., Bujan, S., & Poppeschi, C. (2018).  
855 Spatial and temporal patterns of shoreline change of a 280-km high-energy disrupted sandy coast from  
856 1950 to 2014: SW France. *Estuarine, Coastal and Shelf Science*, 200, 212-223.

857 Coco, G., Senechal, N., Rejas, A., Bryan, K. R., Capo, S., Parisot, J. P., J.A.Brown, MacMahan, J. H.  
858 (2014). Beach response to a sequence of extreme storms. *Geomorphology*, 204, 493-501.

859 De Winter, R. C., Gongriep, F., & Ruessink, B. G. (2015). Observations and modeling of alongshore  
860 variability in dune erosion at Egmond aan Zee, the Netherlands. *Coastal Engineering*, 99, 167-175.

861 Dissanayake, P., Brown, J., and Karunarathna, H., 2015. Impacts of storm chronology on the  
862 morphological changes of the Formby beach and dune system, UK, *Nat. Hazards Earth Syst. Sci.*, 15,  
863 1533-1543, <https://doi.org/10.5194/nhess-15-1533-2015>, 2015.

864 Doyle, T. B., & Woodroffe, C. D. (2018). The application of LiDAR to investigate foredune morphology  
865 and vegetation. *Geomorphology*, 303, 106-121.

866 Esteves, L.S., Brown, J., Williams, J.J., Lymbery, G. (2012). Quantifying thresholds for significant dune  
867 erosion along the Sefton coast, Northwest England. *Geomorphology* 143144, 52–61.

868 Gonçalves, J. A., & Henriques, R. (2015). UAV photogrammetry for topographic monitoring of coastal  
869 areas. *ISPRS Journal of Photogrammetry and Remote Sensing*, 104, 101-111.

870 Hesp, P. (2002). Foredunes and blowouts: initiation, geomorphology and  
871 dynamics. *Geomorphology*, 48(1-3), 245-268.

- 872 Houser, C., Hapke, C., & Hamilton, S. (2008). Controls on coastal dune morphology, shoreline erosion  
873 and barrier island response to extreme storms. *Geomorphology*, 100(3-4), 223-240.
- 874 Houser, C., & Hamilton, S. (2009). Sensitivity of post-hurricane beach and dune recovery to event  
875 frequency. *Earth Surface Processes and Landforms*, 34(5), 613-628.
- 876 Houser, C. (2013). Alongshore variation in beach–dune morphology: implications for barrier island  
877 response. *Geomorphology* 199, 48–61.
- 878 Houser, C., Wernette, P., Rentschlar, E., Jones, H., Hammond, B., & Trimble, S. (2015). Post-storm  
879 beach and dune recovery: Implications for barrier island resilience. *Geomorphology*, 234, 54-63.
- 880 Idier, D., Castelle, B., Charles, E., & Mallet, C. (2013). Longshore sediment flux hindcast: spatio-  
881 temporal variability along the SW Atlantic coast of France. *Journal of Coastal Research*, 65(sp2), 1785-  
882 1790.
- 883 Irish, J. L., & White, T. E. (1998). Coastal engineering applications of high-resolution lidar  
884 bathymetry. *Coastal Engineering*, 35(1-2), 47-71.
- 885 Keijsers JGS, Poortinga A, Riksen MJPM, Maroulis J (2014) Spatio-Temporal Variability in Accretion  
886 and Erosion of Coastal Foredues in the Netherlands: Regional Climate and Local Topography. *PLoS*  
887 *ONE* 9(3)
- 888 Keijsers, J. G. S., De Groot, A. V., & Riksen, M. J. P. M. (2015). Vegetation and sedimentation on  
889 coastal foredues. *Geomorphology*, 228, 723-734.
- 890 Komar, P.D. (1971). Nearshore cell circulation of the formation of giant cusps. *Geol. Soc. Amer. Bull.*  
891 82, 2643-2650.
- 892 Le Mauff, B., Juigner, M., Ba, A., Robin, M., Launeau, P., & Fattal, P. (2018). Coastal monitoring  
893 solutions of the geomorphological response of beach-dune systems using multi-temporal LiDAR  
894 datasets (Vendée coast, France). *Geomorphology*, 304, 121-140.
- 895 Le Nindre Y.M., Benhammouda S., Rouzeau O., Haas H., Quessette J.A. (2001) - Elaboration d'un outil  
896 de gestion prévisionnelle de la côte Aquitaine. Phase 3 : diagnostic d'évolution et recommandations.  
897 Contribution du BRGM, BRGM/P-0822-FR, 115p., 55 fig., 5 tabl., 2 ann.
- 898 Masselink, G., Castelle, B., Scott, T., Dodet, G., Suanez, S., Jackson, D., & Floc'h, F. (2016). Extreme  
899 wave activity during 2013/2014 winter and morphological impacts along the Atlantic coast of  
900 Europe. *Geophysical Research Letters*, 43(5), 2135-2143.
- 901 Matias, A., Ferreira, Ó., Dias, J. A., & Vila-Concejo, A. (2004). Development of indices for the  
902 evaluation of dune recovery techniques. *Coastal Engineering*, 51(3), 261-276.
- 903 Nicolae Lerma, A., Bulteau, T., Lecacheux, S., & Idier, D. (2015). Spatial variability of extreme wave  
904 height along the Atlantic and channel French coast. *Ocean Engineering*, 97, 175-185.
- 905 Nicolae Lerma, A., Bulteau, T., Muller, H., Decarsin, C., Gillet, R., Paris, F., Biauxque M.,  
906 Senechal, N. & Castelle, B. (2018). Towards the Development of a Storm Erosion EWS for the French  
907 Aquitaine Coast. *Journal of Coastal Research*, 85(sp1), 666-670.
- 908 Ollerhead, J., Davidson-Arnott, R., Walker, I. J., & Mathew, S. (2013). Annual to decadal  
909 morphodynamics of the foredune system at Greenwich Dunes, Prince Edward Island, Canada. *Earth*  
910 *Surface Processes and Landforms*, 38(3), 284-298.
- 911 Orzech, M. D., Reniers, A. J. H. M., Thornton, E. B. & MacMahan, J. H. (2011). Megacusps on rip  
912 channel bathymetry: Observations and modeling. *Coastal Engineering*, 58, 890-907.

- 913 Pastol, Y. (2011). Use of airborne LIDAR bathymetry for coastal hydrographic surveying: the French  
914 experience. *Journal of Coastal Research*, 6-18.
- 915 Pedreros, R. (2000). Quantification et modélisation du transport éolien au niveau des zones côtières:  
916 application au littoral girondin (Doctoral dissertation, Bordeaux 1).
- 917 Phillips, M. S., Harley, M. D., Turner, I. L., Splinter, K. D., & Cox, R. J. (2017). Shoreline recovery on  
918 wave-dominated sandy coastlines: the role of sandbar morphodynamics and nearshore wave  
919 parameters. *Marine Geology*, 385, 146-159.
- 920 Pye, K., & Blott, S. J. (2016). Assessment of beach and dune erosion and accretion using LiDAR: impact  
921 of the stormy 2013–14 winter and longer term trends on the Sefton Coast, UK. *Geomorphology*, 266,  
922 146-167.
- 923 Pye, K., Neal, A. (1994). Coastal dune erosion at Formby Point, north Merseyside, England: causes and  
924 mechanisms. *Mar. Geol.* 119, 39–56.
- 925 Richter, A., Faust, D., & Maas, H. G. (2013). Dune cliff erosion and beach width change at the northern  
926 and southern spits of Sylt detected with multi-temporal Lidar. *Catena*, 103, 103-111.
- 927 Sallenger Jr, A. H., Krabill, W. B., R. N. Swift, J. Brock, J. List, Mark Hansen., Holman R. A, Manizade  
928 S., Sontag J., Meredith A., Morgan K., Yunkel J. K., Frederick E. B. and Stockdon H. (2003). Evaluation  
929 of airborne topographic lidar for quantifying beach changes. *Journal of Coastal Research*, 125-133.
- 930 Sallenger, A.H., 2000. Storm impact scale for barrier islands. *J. Coast. Res.* 16, 890–895.
- 931 Saye, S. E., Van der Wal, D., Pye, K., & Blott, S. J. (2005). Beach–dune morphological relationships  
932 and erosion/accretion: an investigation at five sites in England and Wales using LIDAR  
933 data. *Geomorphology*, 72(1-4), 128-155.
- 934 Schupp, C. A., McNinch, J. E., & List, J. H. (2006). Nearshore shore-oblique bars, gravel outcrops, and  
935 their correlation to shoreline change. *Marine Geology*, 233(1-4), 63-79.
- 936 Scott, T., Masselink, G., O'Hare, T., Saulter, A., Poate, T., Russell, P., M. Davidson, Conley, D. (2016).  
937 The extreme 2013/2014 winter storms: Beach recovery along the southwest coast of England. *Marine*  
938 *Geology*, 382, 224-241.
- 939 Senechal, N., Coco, G., Castelle, B., & Marieu, V. (2015). Storm impact on the seasonal shoreline  
940 dynamics of a meso-to macrotidal open sandy beach (Biscarrosse, France). *Geomorphology*, 228, 448-  
941 461.
- 942 Splinter, K.D., Carley, A., Golshani, A., Tomlinson, R. (2014). A relationship to describe cumulative  
943 impact of storm clusters on beach erosion. *Coast. Eng.* 83, 49–55.
- 944 Stockdon, H. F., Holman, R. A., Howd, P. A., & Sallenger Jr, A. H. (2006). Empirical parameterization  
945 of setup, swash, and runup. *Coastal engineering*, 53(7), 573-588.
- 946 Thornton, E. B., MacMahan, J., & Sallenger Jr, A. H. (2007). Rip currents, mega-cusps, and eroding  
947 dunes. *Marine geology*, 240(1-4), 151-167.
- 948 Tucker, M.J. and Pitt, E.G. (2001). Waves in ocean engineering, In Bhattacharyya, R.; McCormick,  
949 M.E. (1st ed.). Oxford: Elsevier. pp. 35–36.
- 950 Turner, I. L., Harley, M. D., & Drummond, C. D. (2016). UAVs for coastal surveying. *Coastal*  
951 *Engineering*, 114, 19-24.
- 952 Vellinga, P. (1982). Beach and dune erosion during storm surges. *Coast. Eng.* 6, 361–367.

953 Vousdoukas, M. I., Almeida, L. P. M., & Ferreira, Ó. (2012). Beach erosion and recovery during  
954 consecutive storms at a steep-sloping, meso-tidal beach. *Earth Surface Processes and Landforms*, 37(6),  
955 583-593.

956 Wang, P., Kirby, J. H., Haber, J. D., Horwitz, M. H., Knorr, P. O., & Krock, J. R. (2006). Morphological  
957 and sedimentological impacts of Hurricane Ivan and immediate poststorm beach recovery along the  
958 northwestern Florida barrier-island coasts. *Journal of Coastal Research*, 1382-1402.

959 Woolard, J. W., & Colby, J. D. (2002). Spatial characterization, resolution, and volumetric change of  
960 coastal dunes using airborne LIDAR: Cape Hatteras, North Carolina. *Geomorphology*, 48(1-3), 269-  
961 287.

962

963

964

965

966

967

968 **Tables:**

969

*Table 1: Nearshore system and beach-dune main characteristics along the Aquitaine coast*

Cell	Nearshore bar system	Outer bar shape	Outer bar length	Inner shape	Inner bar (bar rip channel) length	Berm	Beach width	Beach/dune contact	granulometry	Dune height	Dune evolution scenario / or / System evolution
Cell 1	unpronounced	-	-	-	Temporal	No / small (~0.5m)	20 m	Dune scarp and paleosoil	Sand	10 to 15 m	Natural and fixed (protection). Strong erosion (>2m/y)
Cell 2	uniform longshore bars	straight	-	Straight with unpronounced transverse rip channel	-	No / small (~0.5m)	20 to 40 m)	Dune scarp and paleosoil	Gravel / sand	15 to 20 m	Low erosion (~1m/y)
Cell 3	Double bars	Crescentic and tridimensional	600 - 1 000 m	Almost periodic, deep transverse rip channel	200 to 400 m	North : not established (~0.5m) or small (~0.5m) ? South : Crescentic	100 to 200 m	Rare to frequent established foredune	sand	12 to 25 m	North: strong erosion (>2m/y) South: low erosion (1m/y)
Cell 4	variable	-	-	-	-	Variable	Highly variable	Beach scarp to established foredune	Sand	15 to 25 m	Tidal delta dynamics / sandspit : variable evolution potentially strong erosion (>2m/y)
Cell 5	Double or triple bars	Crescentic and tridimensional	800 - 1200 m	Periodic, deep transverse rip channel	200 to 500 m	Crescentic	200-300 m	Frequent established foredune	Sand	15 to 25 m	Low erosion or stable (<2m/y)
Cell 6	Double bars	cresentic	Irregular, 400-1000 m	Almost perpendicular rip channel	Irregular	Crescentic, frequently doubled	100-120 m	Beach scarp to established foredune	Sand / Coarse sand	15 to 20 m	North: high erosion (>2m/y) South: low erosion (1m/y), locally stable
Cell 7	Double bars	straight	-	Straight with perpendicular rip channel		No / small (~0.5m)	150 to 200 m	Artificialized	Gravel / sand	10 to 15 m	Beach stable, subtidal beach in erosion

970

971

972

973

974

*Table 2: LiDAR campaigns*

<b>Campaign</b>	<b>Date of the survey</b>	<b>Altimetric estimated error Z (m)</b>
LiDAR 2011	5 March to 21 May 2011	0.196
LiDAR 2014	23 - 24 October 2014	0.144
LiDAR 2016	29 - 30 October 2016	0.106
LiDAR 2017	4 - 6 and 7 October 2017	0.102

975

976

977 *Table 3: Rates of coastline evolution along the Aquitaine coast at pluri-annual, decadal and pluri-decadal time scales, in m/year*

Data	Cell 1	Cell 2	Cell 3	Cell 4	Cell 5	Cell 6
LiDAR (2011-2017)	-4.2	-1.4	-0.7	-1.0	-0.1	-1.7
D-GPS (2006-2017)	-5.3	-4.5	-1.0	-2.5	-0.4	-3.5
Orthophotography (1985-2014) Mean trend	-2.5	-1.1	-0.9	-2.5	-0.5	-1.7
Orthophotography (1985-2014) Mean trend - std	-0.5	-0.9	-0.4	-0.8	-0.3	-0.9
Orthophotography (1985-2014) Mean trend + std	-4.5	-1.3	-1.4	-4.1	-0.8	-2.6

978